ANNULAR HEAT TRANSFER WITH SIMULTANEOUSLY DEVELOPING VELOCITY AND TEMPERATURE PROFILES

by 5 2 3

KHANH-DAN HA

B.S., Cheng Kung University, 1966

A MASTER'S THESIS

submitted in partial fulfillment of the

requirements for the degree

MASTER OF SCIENCE

Department of Chemical Engineering

KANSAS STATE UNIVERSITY

Manhattan, Kansas

1969

Approved by:

John C. Matthews

Major Professor

TABLE OF CONTENTS

LIST OF FIGURES

LIST OF TABLES

CHAPTER I

INTRODUCTION

Forced convection heat transfer to fluids flowing in conduits has been of interest in chemical engineering practice for many years. Heat exchangers and cooling coils, two very common devices, both transfer heat, in part if not totally, by forced convection. In forced convection heat is transferred by simultaneous conduction and fluid flow, the pattern of which is determined by an external force as might be exerted by a pump impeller.

The rate of heat transfer in conduits is not uniform, but is greater near the entrance where the velocity and temperature profiles are developing. The nature and rate of these developing profiles depend primarily on the Reynolds number as well as the Prandtl number. A majority of the published annular heat transfer work assumes uniform temperature and fully developed velocity profile at the entrance ($z=0$) and therefore results in reasonably simple governing equations. In the present analysis, the rate of heat transfer is calculated for laminar flow in an annulus with simultaneously developing velocity and temperature profiles. The boundary layer assumptions have been made so that the work is confined to a region between creeping, or very slow flow, and turbulent flow.

It is well known from boundary layer theory that upon entering a conduit a fluid undergoes a velocity development during its course through the conduit. Longitudinally growing boundary layers are formed on each of the boundary surfaces. The thicknesses of these layers increase as the fluid progresses downstream until a point is reached where the boundary layer on one surface intercepts that from the opposite surface. From this point

onward (at a certain value of z), the velocity profile will remain unchanged with further increases in the downstream distance and is then considered to be fully developed.

The temperature profile develops more or less in the same manner except it should be mentioned that it depends to a great extent on the velocity profile. This influence is indicated by the presence of the velocity terms in the differential energy equation. On the other hand, it is not so apparent that the velocity profile is influenced by the temperature profile. In fact, the momentum equation does not contain temperature explicitly, but it does contain temperature-dependent terms such as viscosity.

The determination of the velocity and temperature profiles involves solution of the differential mass, energy and momentum balances. As is often the case, analysis of systems of engineering interest results in very complex partial differential equations, analytical solutions of which exist only for simplified cases. In other words, assumptions have to be made to reduce the problem to a tractable level. In this study, a numerical approach has been used exclusively. Careful assumptions have been made to render the problem soluble, but without oversimplication.

It is assumed herein that the fluid properties are constant and that the velocity and temperature are uniform at the entrance cross section. The study is also restricted to the consideration of incompressible, laminar, Newtonian flow with negligible axial conduction and viscous dissipation. Two distinct problems with various values of the Prandtl number and of the ratio of the inner and outer radii are considered:

(i) For $z > 0$, constant wall temperature at the inner wall and outer wall insulated

(ii) For $z > 0$, uniform heat flux at the inner wall and insulation at the outer wall.

The assumption of constant physical properties avoids coupling of the momentum equation to the energy equation and therefore permits determination of the velocity profile independently. Once the flow pattern is known, the temperature distribution can be calculated.

It is the purpose of this work to study the variation of the Nusselt number with the axial distance from the inlet ($z=0$). Unfortunately, due to the non-linearity of the equation of motion, there is no known analytical method of solution. Two approximate methods involving linearizing the momentum equation have been employed by previous investigators of this problem. The fluid is first assumed to enter the conduit with a constant velocity parallel to its axis. With this initial velocity, the momentum equation is linearized either by Targ's approximation or by applying the technique of Langhaar. The resulting simplified equation can then be solved, often by analytical methods.

No linearization has been attempted in this study. Instead, the finite difference technique has been adopted and the non-linear terms in the equation of motion retained. In this method, the partial derivatives are replaced by difference quotients in the independent variables and the result used as an approximation of the derivatives. The partial differential equations are then reduced to sets of simultaneous algebraic equations which can be solved with the aid of high-speed digital computers.

As a consequence of the boundary layer assumptions the Reynolds number no longer appears as a parameter. It should be borne in mind, however, that the assumptions made in obtaining the boundary layer equations for

this system are satisfied with an increasing accuracy as the Reynolds number increases. Unlike a study with fully developed velocity profile, the Prandtl number becomes of great significance when both profiles are developing simultaneously. Being the ratio of momentum and thermal diffusivity, it provides a measure of the relative rate of formation of the momentum and thermal boundary layers. At a Prandtl number of 10, for example, the rate of momentum diffusion is greater than that of thermal diffusion, with the result that the velocity profile approaches its fully-developed pattern more rapidly than does the temperature profile. On the contrary, for a small Prandtl number, say 0.01, the temperature profile is established much faster. For Prandtl numbers near unity, both velocity and temperature develop at a similar rate. In short, the solutions for uniform velocity profile, $Pr = 0$, and for fully-developed velocity profile, $Pr = \infty$, correspond to the upper and lower limits.

Another important parameter is the ratio of the inner to the outer radius of the annulus. A ratio of zero gives tubular flow while a ratio of unity corresponds to the parallel-plate flow. These two cases, which represent the upper and lower limits of annular flow, have long been studied by many investigators. In fact, if the limit of the annular flow solution is taken as this parameter tends to zero, it is obvious that the solution will not approach that of tubular flow, because for annular flow, an entirely different boundary condition applies at the inner wall.

In this analysis, cases for which the Prandtl number takes on values of 0.01, 1 and 10 and for which the radius ratio takes on values of 2.0 and 10.0 are studied for the two sets of boundary conditions.

CHAPTER II

LITERATURE SURVEY

The important problem of incompressible laminar flow in the entrance region of a circular tube has been studied by many investigators from the points of view of both momentum and energy transport. A number of these papers and those for other geometries as well are given in Ref. (22). In recent years, the annulus problem has also gained increased significance in a number of engineering developments such as the cooling of high-temperature atomic reactors. However, due to the complexity of the governing differential equations, the problem of simultaneously developing velocity and temperature distributions in the entrance region of an annulus has received much less attention. Only a few papers pertinent to the work have been published to date. In the discussion below, the literature surveyed will be divided into three categories, namely (i) the velocity profile, (ii) the temperature profile and (iii) simultaneous development of velocity and temperature profiles. The mathematical techniques involved will be outlined when necessary.

Various approximate solution methods have been devised in the past for determining the laminar flow development of a viscous incompressible fluid in the entrance region of a conduit and can be applied to an annulus. The method of linearization was first originated by Targ (1) in obtaining the developing velocity profile in a flat duct and a tube. It was assumed that the fluid entered the duct with a uniform velocity and that the transverse velocity was of negligible magnitude. It was further assumed that the nonlinear convective term could be replaced by the product of the initial velocity and the velocity gradient in the axial direction. As a result, the

inertial terms of the Navier-Stokes equation were linearized and a linear momentum equation obtained. A number of investigators have applied this technique of Targ's to the developing flow in the hydrodynamic entrance region of annular ducts; among them are Chang and Atabek (2), Roy (3) and Sparrow and Lin (4). The latter workers solved the linearized momentum equation analytically and expressed their results in terms of modified Bassel's functions.

Another important approximate method of solution is due to Langhaar (5), who obtained steady flow patterns in the transition length of a straight tube by means of a linearizing procedure. He introduced the assumption that the convective terms in the boundary layer equation were equal to the product of the kinematic viscosity μ, a parameter β which is a function only of the axial distance, and the axial velocity $v_z(r,z)$ that changed with the axial and radial coordinates z and r. This assumption reduced the momentum equation to a linear form and thus permitted its solution by analytical methods. By application of this technique, Sugino (6) and Reynolds et al. (7) have obtained analytical velocity profiles for the developing annular flow problem. A third method based on a series solution, has been used by Murakawa (8) to obtain the velocity distribution, the pressure drop, and the hydrodynamic entry length in an annulus.

Manohar (9), who had noted that considerable difference existed between results obtained by application of the above approximate methods, undertook an exact analysis of the problem. The Navier-Stokes equations were first simplified under the usual boundary layer assumptions and the resulting non-linear differential equations were solved by an implicit finite-difference method. The idea is much the same as this work though Manohar did not

consider the heat transfer problem. Comparisons between Manohar's results and those of this work have been made and will be discussed in later sections.

Very little experimental work has been done on the developing laminar flow in an annulus. Astill (4) has provided some experimental results pertinent to the analysis of Sparrow and Lin. Velocity profiles were measured using air as the fluid and were compared with Sparrow and Lin's theoretical results. Though agreement between experiment and analysis was considered reasonably good, it was reported that the experimental profiles were more skewed than the analytical profiles. These deviations noted in the neighborhood of the walls were explained as being due to inevitable difficulties in measuring small velocities near solid surfaces.

Much work has been done on laminar-flow annular heat transfer during the past decade. Most of the published papers have been concerned with the thermal entrance region where a fully developed velocity profile is assumed at the inlet. For the case of simultaneously developing velocity and temperature profiles in the entrance region of an annulus, however, only a few publications exist.

Lundberg et al. (10) have presented a theoretical as well as experimental analysis for the thermal problem in hydrodynamically developed flow. This included solution of an eigenvalue problem with four different sets of boundary conditions listed below:

(i) step temperature on one wall, with the other wall maintained at the inlet temperature,

(ii) step heat flux on one wall and insulation on the other,

(iii) step temperature on one wall, with the other wall remaining insulated,

(iv) step heat flux on one wall with the opposite wall maintained at the inlet temperature.

These were the four simplest and most fundamental conditions that could be imposed on an annulus. The linearity and homogeneity of the energy equation permits combination of a variety of these conditions. This technique of superposition can be best illustrated by considering some of the rather complex situations. The case of constant heat flux on one wall and step temperature on the other, for example, can be considered as a superposition of conditions (iii) and (iv) while the case of constant heat fluxes specified on both walls required superposition of condition (ii) twice, one imposed on one wall and the second on the other. Viskanta (11) and Hatton and Quarmby (12) have also presented solutions to some of these same problems. Hsu and Huang (13) considered the problem from a slightly different viewpoint. Instead of prescribed wall temperature and heat fluxes, thermal radiation from the walls was considered. Newton's law of cooling was employed and solutions were obtained for cases of unilateral (outer wall insulated) and bilateral radiative transfer and also for the case where radiative heat transfer at the wall and uniform internal heat generation take place simultaneously. Recently, Hong (14) has presented a study of the thermal entrance problem with fully-developed velocity profile for non-Newtonian fluids represented by the power-law model. Analytical solutions were presented for different values of the power-law model indices and of the inner to outer radius ratio.

There are two theoretical as well as experimental works published for the case of simultaneously developing velocity and temperature. Murakawa (8) has presented numerical and experimental results for the case of constant

wall temperature at the inner wall and insulation at the outer wall. Reynolds et al. (7) have presented the results of a four year study of annular heat transfer to Newtonian fluids. Included in their study is a complete analysis of the annular heat transfer problem with simultaneous development of velocity and temperature profiles. The Langhaar's method of linearizing approximation was adopted and the problem solved by an integral method. Results are tabulated for several inner to outer tube radius ratios and Prandtl numbers. Experimental measurements were made using air (Pr = 0.7) and agreement between theory and experiment was considered excellent.

Shohet (15), using a numerical approach, solved a very general annular entry problem that took into account the effect of a magnetic field on an electrically conducting fluid. The governing equations are basically the same as those used in this work except appearing in the momentum and energy equations are several more terms that account for the applied magnetic field. In addition to the Prandtl number and the inner to outer radius ratio, a third parameter, the Eckert number, comes into consideration in this case. Results were presented graphically for several combinations of these parameters.

CHAPTER III

DEVELOPMENT OF THE MATHEMATICAL MODEL AND FINITE DIFFERENCE EQUATIONS

An analysis will be made of the problem of simultaneous development of velocity and temperature profiles in the entrance region of an annulus. The basic governing equations which are used in analyzing the problem will be presented. General forms of these equations will first be introduced and then reduced by means of simplifying assumptions.

1. Mathematical Statement of Problem

The standard equations for solving this type of problem will be used, namely the continuity equation, the momentum equation and the energy equation. In vector form, they are given by

Continuity:

$$\frac{\partial \rho}{\partial t} + \bar{\nabla} \cdot \rho \bar{v} = 0 \tag{1}$$

Momentum:

$$\rho \frac{D\bar{v}}{Dt} = - \bar{\nabla} p - \bar{\nabla} \cdot \bar{\bar{t}} + \rho \bar{g} \tag{2}$$

Energy:

$$\rho C_v \frac{DT}{Dt} = - (\bar{\nabla} \cdot \bar{q}) - T \left(\frac{\partial p}{\partial T}\right)_v (\bar{\nabla} \cdot \bar{v}) - (\bar{\bar{t}} : \bar{\nabla} \bar{v}) \tag{3}$$

where the energy equation is written in terms of the temperature T of the fluid.

Cylindrical polar coordinates r, θ and z will be used, with the z-axis

lying along the axis of the tube and the origin of the coordinate system at the center of the inlet cross section. The annulus, together with the coordinates and the corresponding notation, is shown in Figure 1. Being axially symmetrical, the flow will be independent of θ. Subject to the following assumptions:

(i) The fluid is incompressible with constant physical properties,

(ii) The flow is steady and laminar,

(iii) There is no viscous dissipation,

(iv) Heat conduction in the z-direction is negligible,

these equations reduce to:

Continuity:

$$\frac{1}{r}\frac{\partial}{\partial r}(r\, v_r) + \frac{\partial v_z}{\partial z} = 0 \tag{4}$$

Momentum:

z-component

$$\rho v_r \frac{\partial v_z}{\partial r} + \rho v_z \frac{\partial v_z}{\partial z} = -\frac{\partial p}{\partial z} + \mu\left[\frac{1}{r}\frac{\partial}{\partial r}\left(r\frac{\partial v_z}{\partial r}\right) + \frac{\partial^2 v_z}{\partial z^2}\right] \tag{5}$$

r-component

$$\rho v_r \frac{\partial v_r}{\partial r} + \rho v_z \frac{\partial v_r}{\partial z} = -\frac{\partial p}{\partial r} + \mu\left[\frac{\partial}{\partial r}\left(\frac{1}{r}\frac{\partial}{\partial r}(r v_r)\right) + \frac{\partial^2 v_r}{\partial z^2}\right] \tag{6}$$

Energy:

$$\rho c_p\left[v_r \frac{\partial T}{\partial r} + v_z \frac{\partial T}{\partial z}\right] = k\left[\frac{1}{r}\frac{\partial}{\partial r}\left(r \frac{\partial T}{\partial r}\right)\right] \tag{7}$$

By utilizing an order-of-magnitude analysis, Prandtl was able to simplify

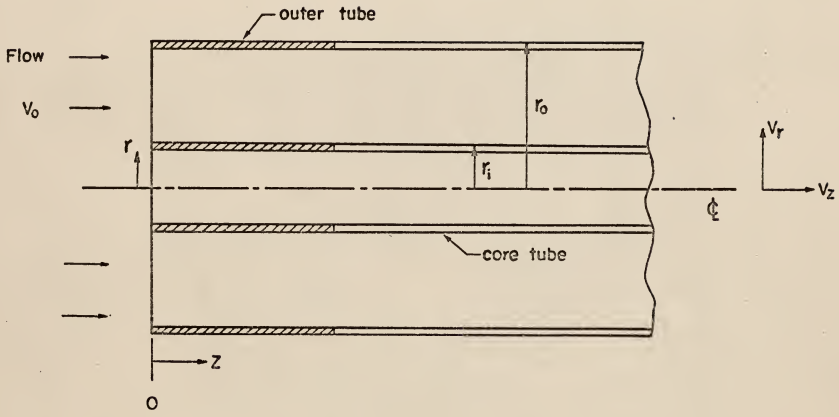

Fig. 1. Diagram of the coordinate system.

the Navier-Stokes equations considerably. Following his arguments, it is possible to drop the term for the molecular transport in the z direction which appears in the z-component of the momentum equation. It is also possible to drop the r-component of the equation completely and assume that the pressure varies only in the z direction. As a result, the number of unknowns has been reduced by one. Applying these assumptions, the governing equations reduce to:

$$\frac{1}{r}\frac{\partial}{\partial r}(rv_r) + \frac{\partial v_z}{\partial z} = 0 \tag{8}$$

$$\rho v_r \frac{\partial v_z}{\partial r} + \rho v_z \frac{\partial v_z}{\partial z} = -\frac{dp}{dz} + \mu\left[\frac{1}{r}\frac{\partial}{\partial r}\left(r\frac{\partial v_z}{\partial r}\right)\right] \tag{9}$$

$$\rho C_p\left[v_r \frac{\partial T}{\partial r} + v_z \frac{\partial T}{\partial z}\right] = k\left[\frac{1}{r}\frac{\partial}{\partial r}\left(r\frac{\partial T}{\partial r}\right)\right] \tag{10}$$

Examination of these equations shows that the temperature variable is present only in the energy equation. Equations (8) and (9) can then be solved simultaneously to give the velocity profile. Once it is known, the temperature profile can be calculated from Equation (10).

2. The Developing Velocity Profile

Assuming that the fluid enters the annulus with a uniform velocity v_o and utilizing the fact that the fluid sticks to the solid surfaces the boundary conditions for Equations (8) and (9) may be written:

$$\begin{array}{llll} z \leq 0, & r_i \leq r \leq r_o, & v_z = v_o, & v_r = 0 \\ z > 0, & r = r_i, & v_z = 0, & v_r = 0 \\ z > 0, & r = r_o, & v_z = 0, & v_r = 0 \end{array} \tag{11}$$

Examination shows that there are two equations with three unknowns, the axial and radial velocities and the pressure. In order to obtain the solution, a third equation is required. As is customarily done, the third equation is obtained from a mass balance between the entrance and an arbitrary distance downstream. The resulting equation is,

$$\int_0^{2\pi}\int_{r_i}^{r_o} \rho v_z r d\theta dr = \rho v_o \pi (r_o^2 - r_i^2) \tag{12}$$

This equation is in fact an integrated form of the equation of continuity. Discussion of the use of this apparently non-independent equation may be found in (16) and (17).

For convenience, the following dimensionless variables are introduced:

$$R = \frac{r}{r_i}$$

$$U = v_z/v_o$$

$$V = v_r/\frac{\mu}{\rho r_i} \tag{13}$$

$$Z = \frac{z}{v_o r_i^2 \rho/\mu}$$

$$P = \frac{p}{\rho v_o^2}$$

The determining equations and the boundary conditions then become

$$\frac{1}{R}\frac{\partial}{\partial R}(RV) + \frac{\partial U}{\partial Z} = 0 \tag{14}$$

$$V\frac{\partial U}{\partial R} + U\frac{\partial U}{\partial Z} = -\frac{dP}{dZ} + \frac{1}{R}\frac{\partial}{\partial R}\left(R\frac{\partial U}{\partial R}\right) \tag{15}$$

$$\int_1^{r_o/r_i} URdR = -\frac{1}{2}\left[\left(\frac{r_o}{r_i}\right)^2 - 1\right] \tag{16}$$

$$\begin{aligned} &Z \leq 0, && 1 \leq R \leq r_o/r_i, && U = 1, && V = 0 \\ &Z > 0, && R = 1, && U = 0, && V = 0 \\ &Z > 0, && R = r_o/r_i, && U = 0, && V = 0. \end{aligned} \tag{17}$$

Note that the only parameter that appears in these equations and the boundary conditions is the radius ratio r_o/r_i. Had the boundary layer assumptions not been introduced, in addition to the ratio r_o/r_i, the Reynolds number would also have appeared as a parameter.

Thus, while considerable mathematical simplification has been achieved, the non-linear character of the Navier-Stokes equation has been preserved. There remains a system of three simultaneous equations to be solved for the three unknowns U, V and P.

A. The Finite-Difference Technique

Only a small fraction of the partial differential equations generated in engineering problems can be solved by formal analytical methods. With the non-linearity of the momentum equation retained, only a numerical solution can be provided. The finite-difference technique will be employed in this work. By using difference equations in place of the derivatives in the partial differential equations, the problem can be reduced to solving sets of algebraic equations.

To elucidate the nature of this method, consider a mesh network imposed on the annulus as shown in Figure 2. The mesh covers the entire cross section of the annulus and continues as far from the entrance as is necessary.

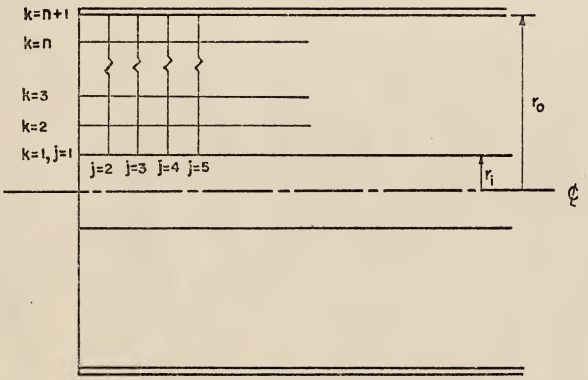

Fig. 2. Mesh network for finite difference representations.

Since the equation is independent of θ, it is understood that the mesh network applies to all planes normal to the walls. As a general rule, the more the mesh is refined, the smaller the truncation error, that is, the smaller the error associated with determining the expressions for the derivatives from only a few terms of the Taylor series.

Equations (14) and (15) can be rewritten as

$$\frac{\partial}{\partial R}(RV) + R\frac{\partial U}{\partial Z} = 0 \tag{18}$$

$$V\frac{\partial U}{\partial R} + U\frac{\partial U}{\partial Z} = -\frac{dP}{dZ} + \frac{\partial^2 U}{\partial R^2} + \frac{1}{R}\frac{\partial U}{\partial R} \tag{19}$$

The following difference quotients will be used for the derivatives in these equations:

Continuity:

$$\frac{\partial U}{\partial Z} = \frac{U(j+1,k+1) - U(j,k+1) + U(j+1,k) - U(j,k)}{2(\Delta Z)}$$

$$\frac{\partial}{\partial R}(RV) = \frac{R(k+1)V(j+1,k+1) - R(k)V(j+1,k)}{\Delta R} \tag{20}$$

Momentum:

$$\frac{\partial U}{\partial Z} = \frac{U(j+1,k) - U(j,k)}{\Delta Z}$$

$$\frac{\partial U}{\partial R} = \frac{U(j+1,k+1) - U(j+1,k-1)}{2(\Delta R)}$$

$$\frac{\partial^2 U}{\partial R^2} = \frac{U(j+1,k+1) - 2U(j+1,k) + U(j+1,k-1)}{(\Delta R)^2} \tag{21}$$

$$\frac{dP}{dZ} = \frac{P(j+1) - P(j)}{\Delta Z}$$

The difference equations for Equations (18) and (19) at a typical mesh point (j,k) are then

$$\frac{R(k+1)V(j+1,k+1) - R(k)V(j+1,k)}{\Delta R}$$

$$+ \frac{1}{2(\Delta z)} \{R(k+1)[U(j+1,k+1) - U(j,k+1)] + R(k)[U(j+1,k) - U(j,k)]\} = 0 \tag{22}$$

$$V(j,k) \frac{U(j+1,k+1)-U(j+1,k-1)}{2(\Delta R)} + U(j,k) \frac{U(j+1,k)-U(j,k)}{\Delta Z}$$

$$= \frac{P(j)-P(j+1)}{\Delta Z} + \frac{U(j+1,k+1)-2U(j+1,k)+U(j+1,k-1)}{(\Delta R)^2}$$

$$+ \frac{1}{R(k)} \frac{U(j+1,k+1)-U(j+1,k-1)}{2(\Delta R)} \tag{23}$$

After rearrangement they become

$$V(j+1,k+1) = \frac{R(k)}{R(k+1)} V(j+1,k)$$

$$- \frac{\Delta R}{2(\Delta Z)R(k+1)} \{R(k+1)[U(j+1,k+1)-U(j,k+1)]$$

$$+ R(k) [U(j+1,k)-U(j,k)]\} \tag{24}$$

$$C(j,k)U(j+1,k-1) + A(j,k)U(j+1,k) + B(j,k)U(j+1,k+1)$$

$$+ \frac{P(j+1)(\Delta R)^2}{\Delta Z} = E(j,k) \tag{25}$$

where

$$C(j,k) = \frac{\Delta R}{2R(k)} - 1 - \frac{V(j,k)\Delta R}{2}$$

$$A(j,k) = 2 + \frac{(\Delta R)^2}{\Delta Z} U(j,k)$$

$$B(j,k) = \frac{\Delta R}{2} V(j,k) - 1 - \frac{\Delta R}{2R(k)} \qquad (26)$$

$$E(j,k) = \frac{(\Delta R)^2}{\Delta Z} P(j) + \frac{(\Delta R)^2}{\Delta Z} [U(j,k)]^2$$

Equations (24) and (25) can be applied to every interior point k for each column j. Using Equation (25) as an example, the following equations can be written for each k, i.e., k = 2, 3, ..., n:

$$C(j,2)U(j+1,1)+A(j,2)U(j+1,2)+B(j,2)U(j+1,3) + \frac{P(j+1)(\Delta R)^2}{\Delta Z} = E(j,2)$$

$$C(j,3)U(j+1,2)+A(j,3)U(j+1,3)+B(j,3)U(j+1,4) + \frac{P(j+1)(\Delta R)^2}{\Delta Z} = E(j,3) \qquad (27)$$

$$C(j,n)U(j+1,n-1)+A(j,n)U(j+1,n)+B(j,n)U(j+1,n+1) + \frac{P(j+1)(\Delta R)^2}{\Delta Z} = E(j,n)$$

In these equations, U(j+1,1) and U(j+1,n+1) represent the dimensionless axial velocity at the inner and outer wall respectively and both vanish by the second and third boundary conditions of Equation (17). The same is true for V(j+1,1) and V(j+1,n+1) that appear in Equation (24).

The material balance equation, Equation (16), can be approximated by the trapezoidal rule for column j+1 as follows:

$$\int_1^{r_o/r_i} URdR = \Delta R \left\{ \frac{U(j+1,1)R(1)+U(j+1,2)R(2)}{2} + \frac{U(j+1,2)R(2)+U(j+1,3)R(3)}{2} + \text{----------} + \frac{U(j+1,n-1)R(n-1)+U(j+1,n)R(n)}{2} \right\}$$

$$= \Delta R \sum_{k=2}^{n-1} U(j+1,k)R(k)$$

$$= \frac{1}{2}\left[\left(\frac{r_o}{r_i}\right)^2 - 1\right] \qquad (28)$$

where, as before, both U(j+1,1) and U(j+1,n) vanish.

The finite difference approximations, Equations (20) and (21), have been employed successfully by Shohet (15) in obtaining the velocity profile for laminar magnetohydrodynamic flow in the entrance region of an annulus. It has also been shown (18)(19) that such substitutions produce stable difference equations for any selection of the ratio of ΔR and ΔZ.

B. Solution of The Velocity Profile

Equations (27) and (28) constitute a set of linear algebraic equations that can be solved simultaneously to give the pressure and the n+1 values of the axial velocity. The solution was obtained by a trial and error procedure. First, a reasonable value for the pressure P(j+1) in Equation (27) was assumed. The resulting set of n-1 equations with n-1 unknowns were solved by the Thomas method (20). Equation (28) was then used as an equation of constraint. In other words, it was used to determine whether the correct

values of U were obtained. If it was satisfied, by substituting these values of U into Equation (24), the radial velocities could be calculated. Had it not been satisfied, another value for the pressure would have been assumed and the calculation of the U's repeated. Examination of Equation (27) showed that a large assumed value of P(j+1) gave small U's. Thus, if the left hand side of Equation (28) was greater than the right hand side, a smaller P(j+1) was assumed whereas in the case where the left hand side was smaller than the right hand side, a larger P(j+1) would be desired.

To obtain the velocity profile as a function of the axial and radial distances, calculations were started at the j=1 column, corresponding to the entrance of the annulus. Equations similar to (25) were written for each interior point k=2,3, ...,n while Equation (28) was applied to the entire column. The resulting system of n+1 algebraic equations were then solved according to the above procedure. With the newly found axial and radial velocities and the pressure at j=1, calculations could proceed to the j=2 column. In this manner, integration of the momentum equation was completed from j to j+1 and it was possible then to advance column by column along the annulus until the fully developed velocity profile was obtained.

The calculations were performed on a digital computer and the results are presented in Figures 3, 4, 5 and 6 for two different values of the radius ratio, namely r_o/r_i = 2.0 and 10.0. The flow was considered fully developed when the velocity at j and j+1 remained the same to four decimal places.

To avoid propagation of round-off errors in calculating the radial velocity from the known axial velocity, the so-called "biased downward velocity" proposed by Shohet (15) was introduced. Contrary to Equation (24) in which the radial velocity was calculated in an upward direction, i.e., from

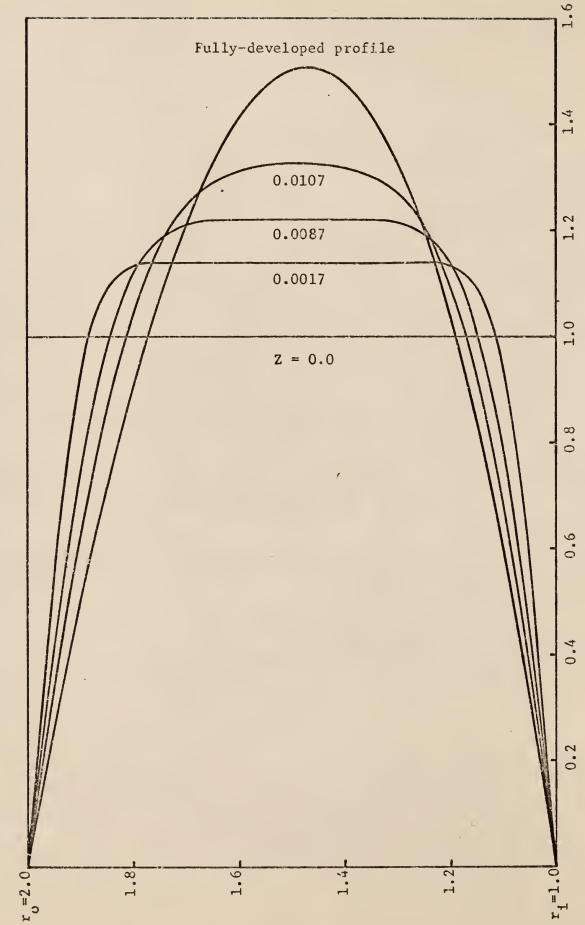

Fig. 3. Developing velocity distribution for $r_o/r_i = 2.0$.

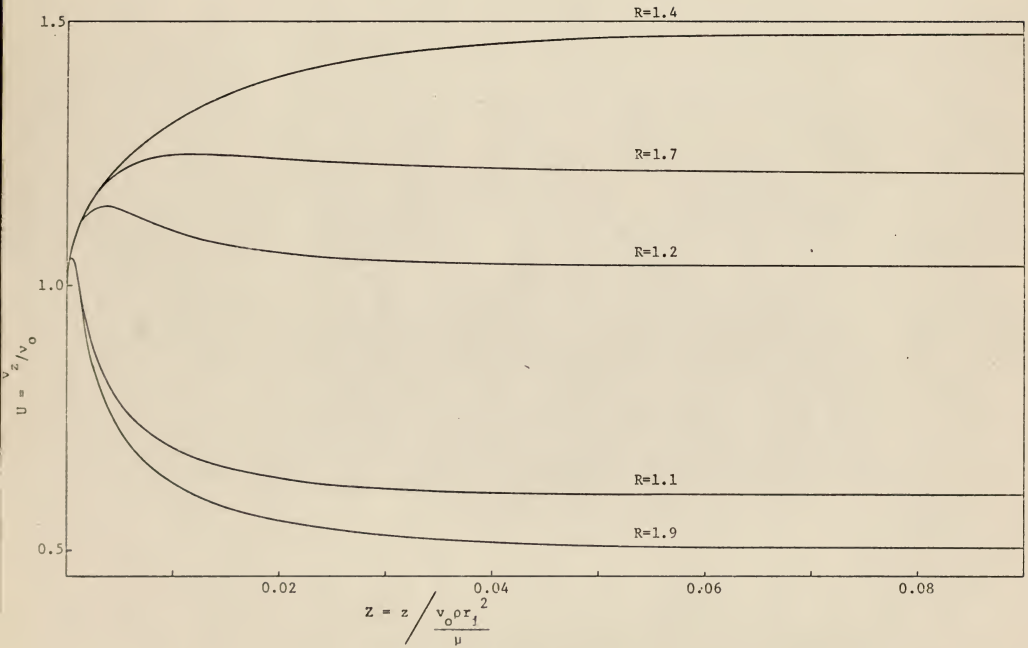

Fig. 4. Developing velocity distribution at various radial positions, $r_o/r_1 = 2.0$.

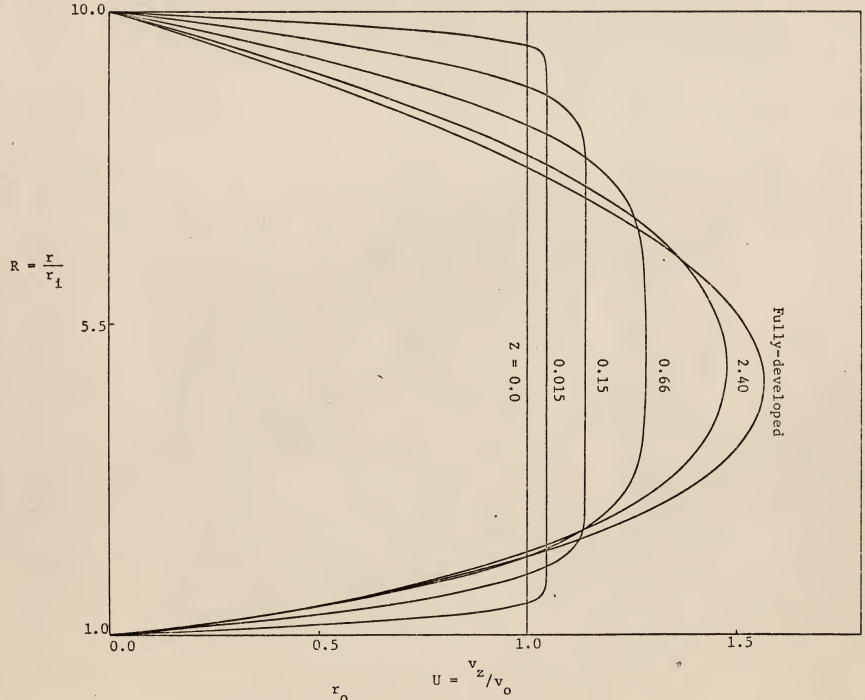

Fig. 5. Developing velocity profiles, $\frac{r_o}{r_i} = 10.0$.

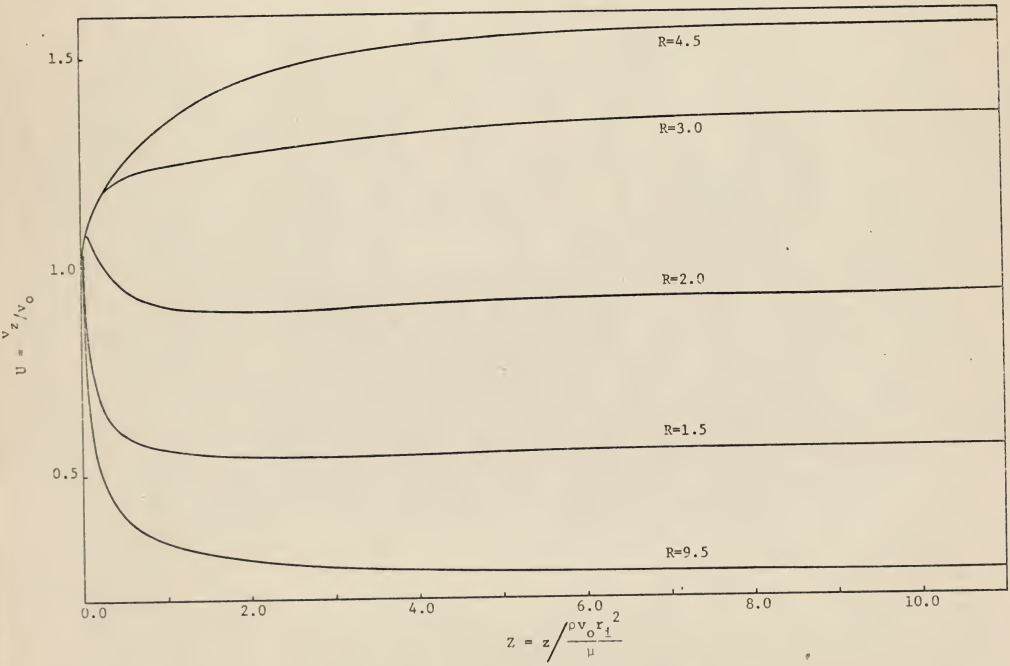

Fig. 6. Developing velocity profiles at various radial positions, $r_o/r_i = 10.0$.

the inner wall to the outer wall of the annulus, the V's were also calculated in a reversed direction. Thus, by substituting the following difference quotients

$$R\frac{\partial U}{\partial Z} = \frac{R(k-1)[U(j+1,k-1)-U(j,k-1)]+R(K)[U(j+1,k)-U(j,k)]}{2(\Delta Z)}$$

$$\frac{\partial}{\partial R}(RV) = \frac{R(k)V(j+1,k) - R(k-1)V(j+1,k-1)}{\Delta R} \qquad (29)$$

into Equation (18), a slightly different form of the continuity equation is obtained:

$$\frac{R(k)V(j+1,k) - R(k-1)V(j+1,k-1)}{\Delta R}$$

$$+ \frac{R(k-1)[U(j+1,k-1)-U(j,k-1)]+R(k)[U(j+1,k)-U(j,k)]}{2(\Delta Z)} = 0$$

After rearrangement, it becomes

$$V(j+1,k-1) = \frac{R(k)V(j+1,k)}{R(k-1)}$$

$$+ \frac{\Delta R}{2\Delta Z R(k-1)} \{R(k-1)[U(j+1,k-1)-U(j,k-1)]$$

$$+ R(k)[U(j+1,k)-U(j,k)]\} \qquad (30)$$

It is of interest to note that by using the same values of the axial velocity calculated from Equation (27), appreciably different results were obtained for the radial velocity from Equations (24) and (30) respectively. Round-off errors were accumulating in opposite directions, i.e., towards the outer wall for equation (24) and towards the inner wall for Equation (30).

If the axial velocities were exact, then within computational error, Equation (24) would give accurate V velocities near the inner wall whereas Equation (30) would give accurate V's near the outer wall. To minimize these round-off errors, the values of the radial velocities calculated both from Equations (24) and (30) were averaged for all but the interior points k=2 and k=n. At these two points, instead of taking the average, the values calculated respectively from Equations (24) and (30) were retained.

As was mentioned earlier, calculation of the axial velocity followed a trial and error procedure in which the macroscopic material balance, Equation (28), was used as a constraint. An allowable error of approximately ±0.01 per cent was imposed upon this equation. To start the calculation, the first problem to be confronted is the value of the axial velocity at points k=1, j=1 and k=n+1, j=1. At an infinitesimal distance preceding these points, the axial velocity is one, whereas at a corresponding infinitesimal distance within the annulus, the axial velocity is zero on the walls. In other words, the flow is discontinuous at these points as the fluid enters the annulus. While there was no information to determine the values of the axial velocity at these points, an average value of 0.5 was assigned.

Another problem is the proper sizes of the mesh network to be imposed upon the annulus. In general, the error committed in replacing the derivatives of the boundary layer equations by difference quotients approached zero as the mesh was refined. Comparisons could be made by using several different mesh networks and the most appropriate one chosen. Different mesh sizes were used along the annulus. For convenience, they are listed in Table 1. Results will be compared with available data in a later section.

Table 1. Mesh sizes for the continuity and momentum equations.

Radius ratio r_o/r_i	Mesh number of R	Z	ΔZ	ΔR
2.0	51	0.0	0.00001	0.02
		0.0015	0.00005	0.02
		0.0108	0.0001	0.02
		0.09	0.0005	0.02
		fully-developed		
10.0	151	0.0	0.00001	0.06
		0.0003	0.00005	0.06
		0.0024	0.0001	0.06
		0.009	0.0002	0.06
		0.045	0.0005	0.06
		0.108	0.001	0.06
		0.3	0.002	0.06
		1.14	0.005	0.06
		3.0	0.01	0.06
		7.8	0.02	0.06
		15.6	0.05	0.06
		fully-developed		

C. The Fully Developed Velocity Profile

The laminar flow fully developed velocity profile in an annulus has been given by a number of investigators. The derivation is presented here for two reasons. First, the definitions of the dimensionless variables in this work are different from those of previous investigators and secondly the equation can be used as a check on the accuracy of the numerical solution.

The appropriate differential equation of motion for fully developed laminar flow is

$$\frac{dP}{dZ} = \frac{1}{R}\frac{d}{dR}\left(R\frac{dU_\infty}{dR}\right) \tag{31}$$

and the boundary conditions are:

$$\begin{aligned} &R = 1, && U_\infty = 0 \\ &R = r_o/r_i, && U_\infty = 0 \\ &R = R_{max}, && \frac{dU_\infty}{dR} = 0 \end{aligned} \tag{32}$$

where U_∞ denotes the fully developed axial velocity, a function only of R.

Integrating Equation (31) twice with respect to R yields

$$U_\infty = \frac{1}{4}\left(\frac{dP}{dZ}\right)R^2 + C_1 \ln R + C_2 \tag{33}$$

in which C_1 and C_2 are constants of integration. Application of the first and third conditions of Equation (32) gives

$$U_\infty = \frac{1}{4}\left(\frac{dP}{dZ}\right)\left(R^2 - 1 - 2R_{max}^2 \ln R\right) \tag{34}$$

whereas application of the second and third conditions leads to

$$U_\infty = \frac{1}{4}\left(\frac{dP}{dZ}\right)\left[R^2 - \left(\frac{r_o}{r_i}\right)^2\right] - \frac{1}{2}\left(\frac{dP}{dZ}\right)R_{max}^2\left[\ln R - \ln\left(\frac{r_o}{r_i}\right)\right] \tag{35}$$

Obviously, Equations (34) and (35) must yield the same axial velocity for all values of R. Thus, equating the two equations will give the position where maximum velocity occurs,

$$R_{max}^2 = \frac{(r_o/r_i)^2 - 1}{2 \ln (r_o/r_i)} \tag{36}$$

The pressure gradient, $\frac{dP}{dZ}$, may be expressed in terms of the average velocity defined by

$$(v_z)_{avg} = v_o = \frac{\int_0^{2\pi}\int_{r_i}^{r_o} v_z \, d\theta dr}{\int_0^{2\pi}\int_{r_i}^{r_o} r \, d\theta dr} \tag{37}$$

Equation (37) can be written in terms of dimensionless variables as

$$1 = \frac{\int_0^{2\pi}\int_1^{r_o/r_i} U_\infty R \, d\theta dR}{\int_0^{2\pi}\int_1^{r_o/r_i} R \, d\theta dR} = \frac{\int_1^{r_o/r_i} U_\infty R \, dR}{\frac{1}{2}\left[(r_o/r_i)^2 - 1\right]} \tag{38}$$

Substitution of Equations (36) and (38) into Equation (34) results in the

following expression for the pressure gradient,

$$\frac{dP}{dZ} = 8/\left\{\frac{(r_o/r_i)^2 - 1}{\ln (r_o/r_i)} - \left(\frac{r_o}{r_i}\right)^2 - 1\right\} \tag{39}$$

Equation (34) can then be written as

$$U_\infty = \frac{2\left[R^2 - 1 - \left\{\left(\frac{r_o}{r_i}\right)^2 - 1\right\} \frac{\ln R}{\ln (r_o/r_i)}\right]}{\left[\frac{(r_o/r_i)^2 - 1}{\ln (r_o/r_i)} - \left(\frac{r_o}{r_i}\right)^2 - 1\right]} \tag{40}$$

The result obtained in Equation (40) can be compared with the numerical solution obtained far from the entrance. The comparisons are made in Table 2 and it can be seen that agreement is excellent.

D. The Pressure Drop

The pressure at any cross section along the annulus was obtained simultaneously with the axial velocity by solving Equations (27) and (28). The pressure drop, which is due to friction at the walls and the change of momentum between the entrance and any downstream cross section, could then be calculated using a constant dimensionless pressure of 10.0 at the inlet. With an allowable error of approximately ±0.01 percent the pressure could be calculated to the fourth significant figure. Results are presented graphically in Figures 7 and 8. It will be seen in a later section that the pressure drop is not only a function of the dimensionless distance but also depends on the radius ratio and decreases with increase in the value of the ratio.

E. The Entrance Length

An estimate of the hydrodynamic entrance length may be made on the basis

Table 2. Analytical and numerical fully-developed velocity profiles for r_o/r_i = 2.0 and 10.0.

	Radial positions	Fully-developed velocity U	
	R	analytical	numerical
r_o/r_i = 2.0	1.0	0.0	0.0
	1.1	0.603	0.6033
	1.2	1.039	1.0396
	1.3	1.325	1.3267
	1.4	1.477	1.4778
	1.471 (R_{max})	1.5075	1.5079
	1.5	1.502	1.5034
	1.6	1.411	1.4121
	1.7	1.210	1.2108
	1.8	0.904	0.9053
	1.9	0.5	0.5004
	2.0	0.0	0.0
r_o/r_i = 10.0	1.0	0.0	0.0
	1.5	0.558	0.5569
	2.0	0.924	0.9247
	3.0	1.353	1.352
	4.0	1.538	1.5378
	4.64 (R_{max})	1.5673	1.5672
	5.0	1.558	1.561
	6.0	1.450	1.4495
	7.0	1.230	1.2299
	8.0	0.911	0.9106
	9.0	0.499	0.4992
	10.0	0.0	0.0

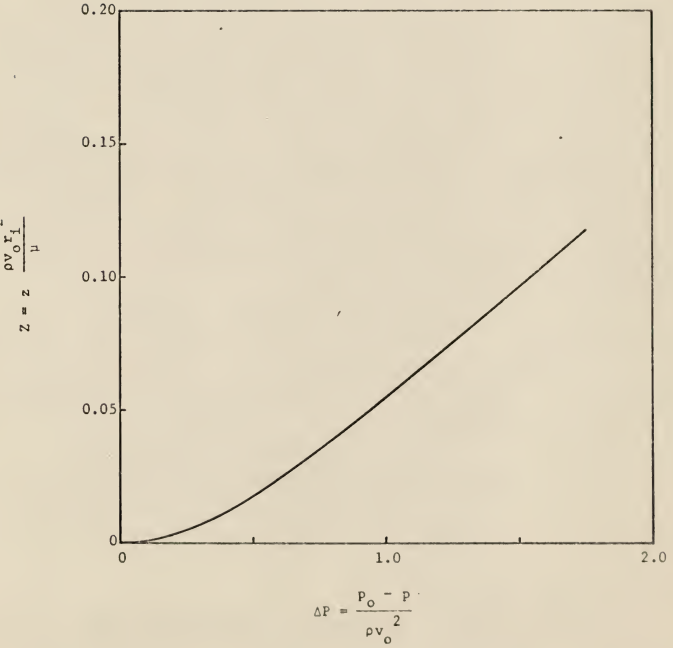

Fig. 7. Pressure drop in the hydrodynamic entrance region, $r_o/r_i = 2.0$.

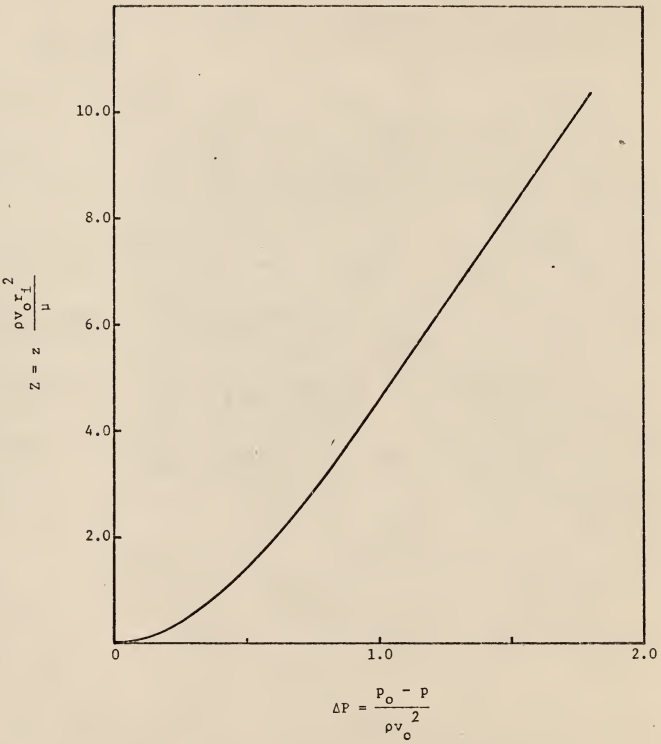

Fig. 8. Pressure drop in the hydrodynamic entrance region, $r_o/r_i = 10.0$.

of the approach of the numerical axial velocity to its fully developed value. The maximum velocity for fully developed flow occurs at a radius $R = R_{max}$ and is given by

$$(U_\infty)_{max} = \frac{2[R_{max}^2 - 1 - \{(\frac{r_o}{r_i})^2 - 1\} \frac{\ln R_{max}}{\ln(r_o/r_i)}]}{[\frac{(r_o/r_i)^2 - 1}{\ln(r_o/r_i)} - (\frac{r_o}{r_i})^2 - 1]} \tag{41}$$

where

$$R_{max}^2 = \frac{(r_o/r_i)^2 - 1}{2 \ln (r_o/r_i)} \tag{36}$$

The entrance length, Z_n, is then defined as the distance at which the maximum velocity attains a particular percentage of the maximum fully developed value, that is

$$\frac{U(Z_n, R_{max})}{(U_\infty)_{max}} = \text{desired percentage.} \tag{42}$$

The entrance lengths for two different values of the radius ratio are calculated and tabulated in Table 3 where the percentage has been chosen as 99%.

F. Results and Discussion

The numerical results of the developing velocity profiles are shown in Figures 3, 4, 5 and 6 corresponding respectively to values of the annulus ratio of $\frac{r_o}{r_i} = 2.0$ and 10.0. The good agreement between the analytical and numerical fully developed profiles has been shown previously in Table 2. To further demonstrate the adequacy of the numerical method employed, results

Table 3. Comparison of entrance lengths.

$\frac{1}{r_o/r_i}$	$Z' = z/\frac{\rho v_o}{\mu}(r_o - r_i)^2$					
	Ha	Manohar (9)	C & A (2)	Roy (3)	Reynolds (7)	Sugino (6)
0.05					0.0704	
0.1	0.0685	0.0654	0.076	0.072	0.0568	
0.2			0.063	0.06325		0.02
0.25					0.0472	
0.3		0.0490	0.057	0.056		
0.4			0.051	0.05125		
0.5	0.0444	0.044		0.0485	0.0404	0.01973
0.6			0.048	0.046		
0.7		0.0411				
0.8			0.047	0.045		

of this work will be compared with those obtained by other methods, whenever they are available.

Shown in Figures 9, 10 and 11 are some of the velocity profiles obtained by a number of investigators. It can be seen that for both values of the radius ratio, the results of Manohar (9), who likewise employed the finite-difference technique, appear to deviate slightly from those of this work. His results are considered to be in error because of the way he handled the corner conditions at the point of entry. The usual treatment assumes that the fluid approaches the entrance with a uniform velocity profile, including the velocity at the wall positions. Manohar, on the other hand, assumed a velocity profile where the velocities were taken to be zero on the boundaries and unity at other mesh points. In other words, the mass flux as a result of his assumption of the inlet conditions is less than usual and consequently leads to the deviation of his results.

The calculated results by Sugino (6) for the case of $\frac{r_o}{r_i} = 2.0$ at $R = 1.5$ are shown in Figure 9 for comparison and his velocity profile appears to develop much faster. The results obtained by Chang and Atabek (2) and by Sparrow and Lin (4) for $\frac{r_o}{r_i} = 10.0$ at various positions are compared in Figure 11. While agreement between Sparrow and Lin's results and that of this work is reasonably good, Chang and Atabek's profiles deviate in the vicinity of the inlet.

So far only the velocity distributions have been discussed. The changes in these profiles along the annulus have an important effect on the pressure drop. As can be seen from Figures 7 and 8, the pressure drop rises sharply in the immediate vicinity of the inlet and grows gradually along the annulus until it finally comes to a constant value when the velocity profile becomes

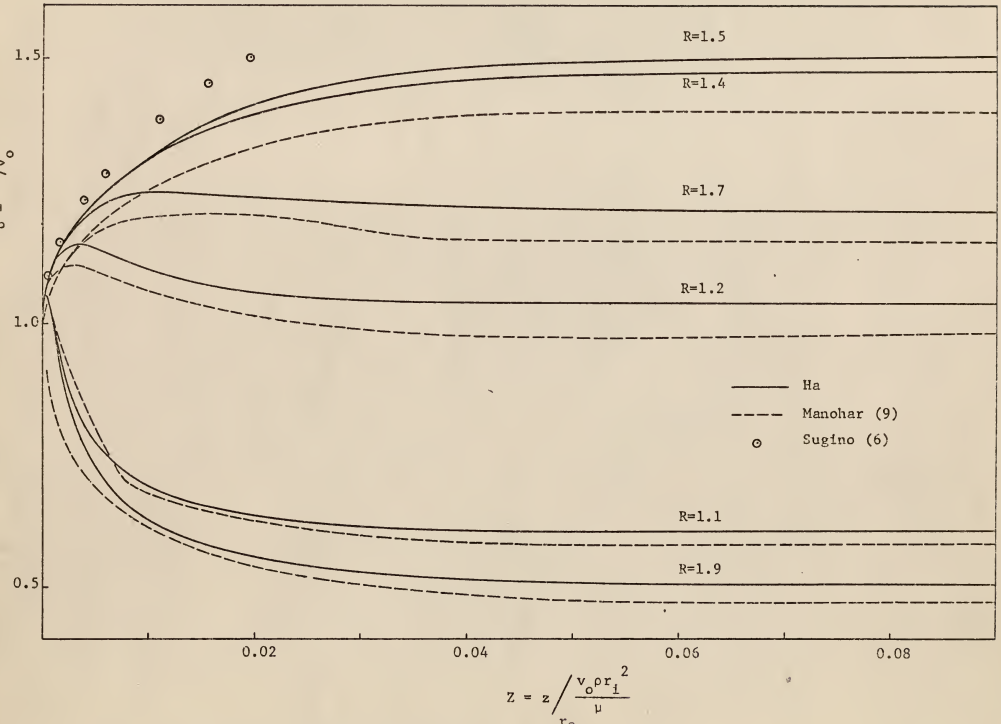

Fig. 9. Comparison of developing velocity profiles, $\frac{r_o}{r_i} = 2.0$.

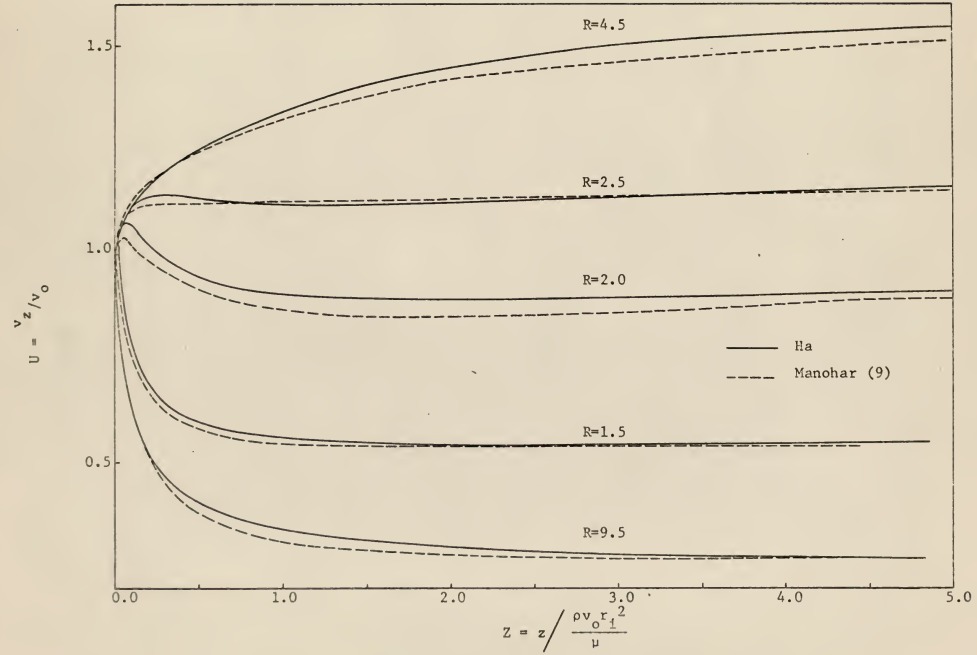

Fig. 10. Comparison of developing velocity profiles I, $r_o/r_1 = 10.0$.

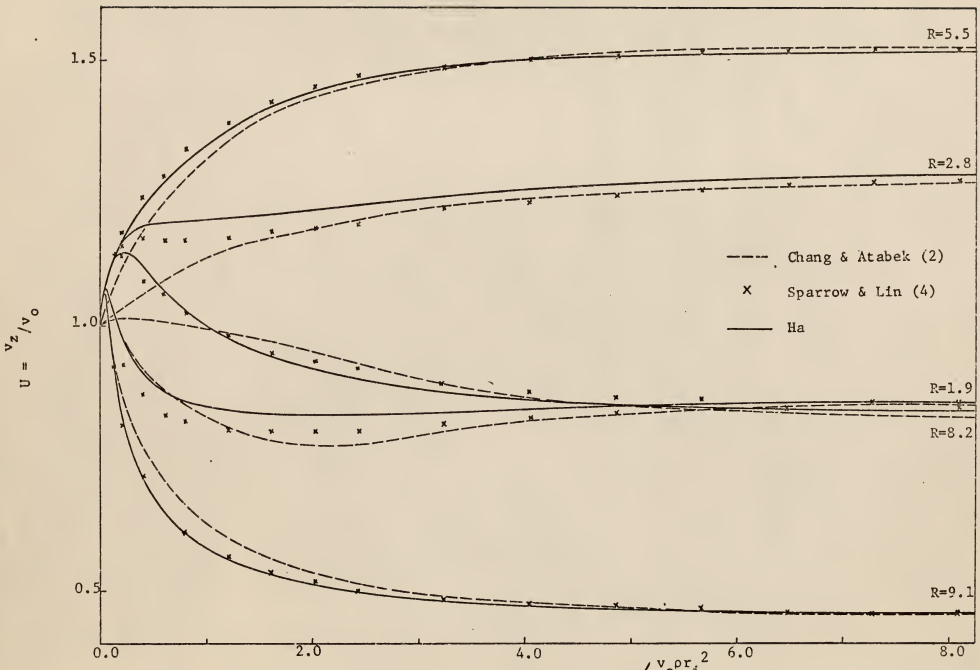

Fig. 11. Comparison of developing velocity profiles II, $r_o/r_i = 10.0$.

fully-developed. Figure 12 shows the pressure drop as a function of the axial distance and the radius ratio, where the axial distance is taken to be $Z' = \frac{Z}{(\frac{r_o}{r_i} - 1)^2}$ for convenience.

A comparison between Manohar's results (9) and those of this work is provided in Figures 13 and 14 corresponding to $\frac{r_o}{r_i} = 2.0$ and 10.0 respectively. Again, Manohar's results appear to be too small and such deviation is believed to result from the inaccuracy of his velocity profiles. The fully-developed pressure gradients are also shown in these Figures. The excellent agreement between analytical and numerical results once again substantiate the accuracy of the finite-difference technique employed. In Figure 15, the pressure drops in the vicinity of the inlet are plotted. While Sugino's results (6) seem to agree with that of this work, the calculated results by Murakawa (8) appear to be too small near the entrance.

The entrance length is defined by Equation (42) in a previous section. Most of the published work provides results with a desired percentage of 99%. Since the methods of defining the dimensionless axial distance by various authors are different, it is necessary to adopt one as a criterion in order to compare their results. As before the dimensionless quantity that takes into account the radius ratio, $Z' = \frac{z}{(r_o - r_i)^2 u_o \rho/\mu} = \frac{Z}{(\frac{r_o}{r_i} - 1)^2}$, is employed.

The results are shown in Figure 16 with Z' plotted against the reciprocal of the radius ratio $\frac{r_o}{r_i}$. Inspection of the figure reveals that the entrance length decreases with the decreasing radius ratio. It also shows that the results obtained by Roy (3) are almost identical to those by Chang and Atabek (2) whereas the results of Manohar (9), Reynolds et al. (7) and this

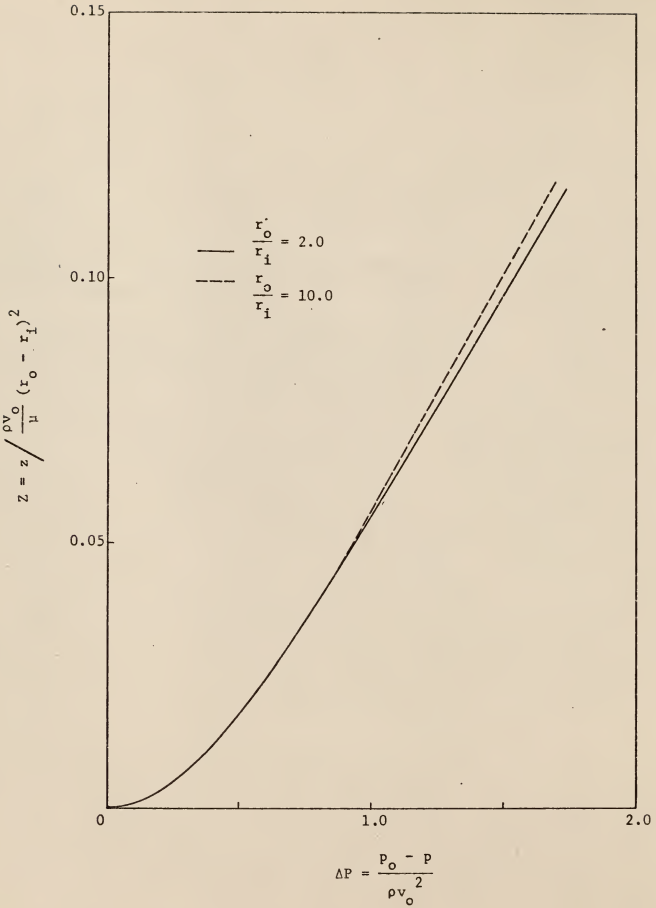

Fig. 12. Pressure drop in the hydrodynamic entrance region.

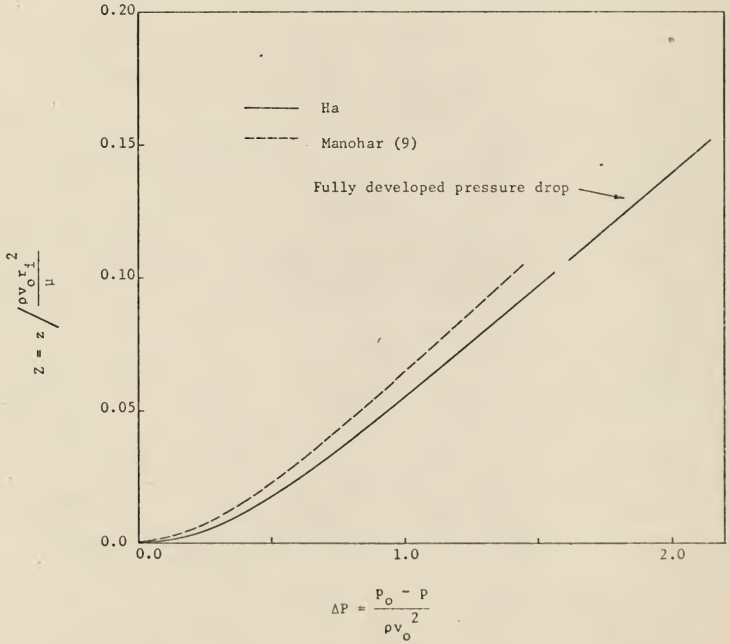

Fig. 13. Comparison of pressure drops in the hydrodynamic entrance region, $r_o/r_i = 2.0$.

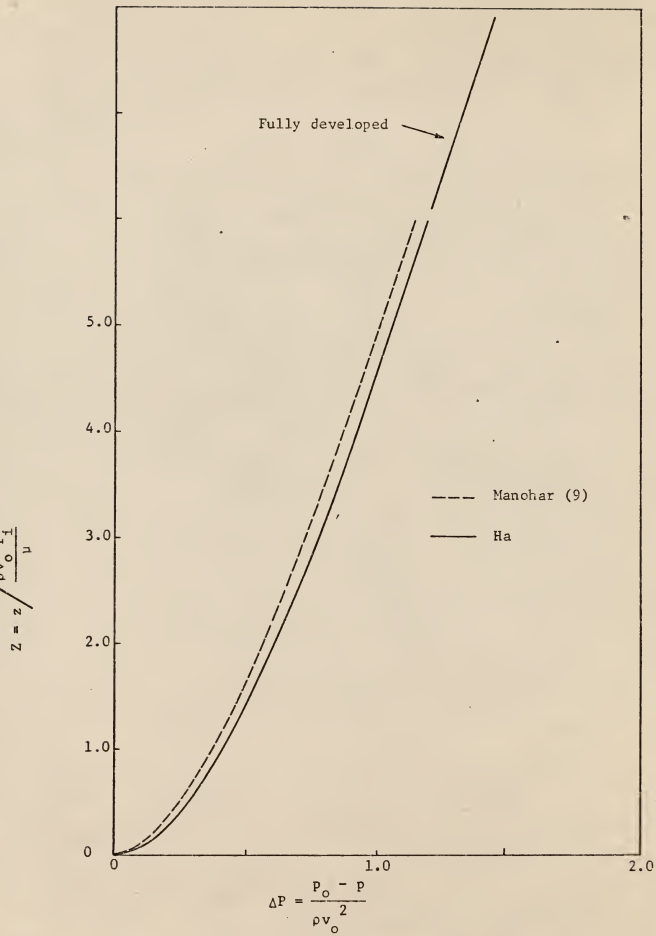

Fig. 14. Comparison of pressure drops in the hydrodynamic entrance region, $r_o/r_i = 10.0$.

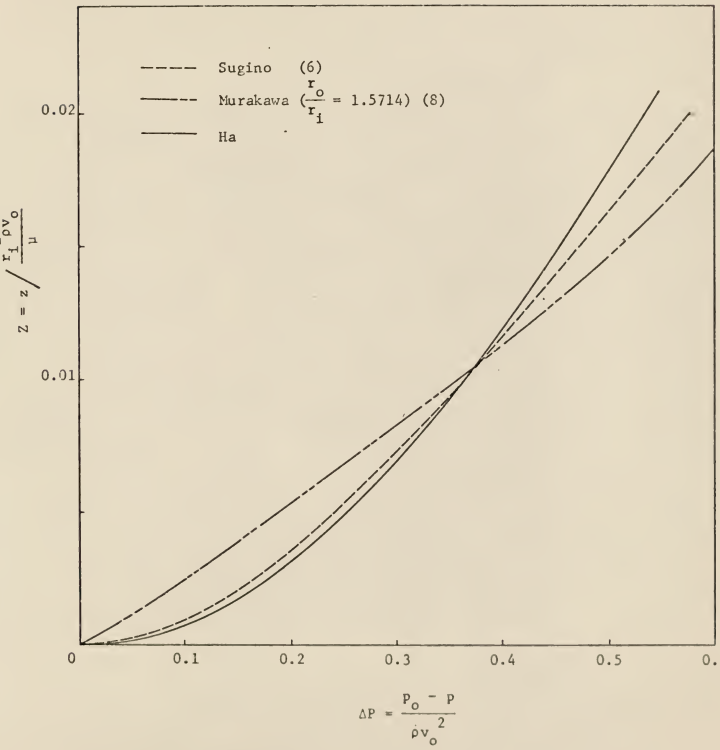

Fig. 15. Pressure drop in the vicinity of the inlet for $\frac{r_o}{r_i}$ = 2.0.

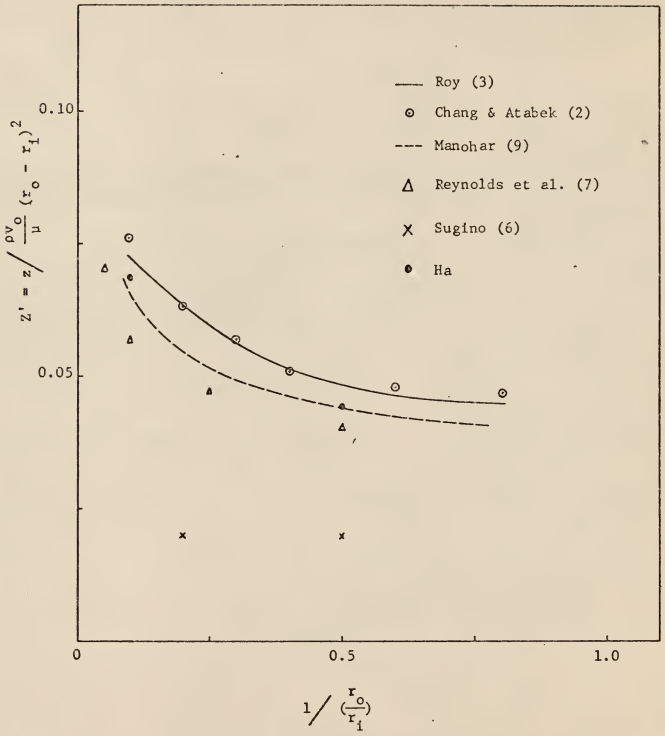

Fig. 16. Comparison of entrance lengths.

work are approximately the same. Sugino (6) concluded in his work that the entrance length was unaffected by the radius ratio r_o/r_i and that it is approximately 0.02. Based on the calculations of this and other work, his conclusion seems in error.

3. The Temperature Profile

The problem of determining the developing temperature profiles in the entrance region of an annulus will be presented in the following sections. With a numerical method of solution, any kind of wall-temperature variation or heating rate can be handled with equal ease. Consideration has been restricted, however, to two distinct limiting cases.

A. Case I: constant temperature at the inner wall, outer wall insulated.

A.1. Mathematical statement of the problem.

The coordinates and geometry of the system have been shown in Figure 1. The fluid flows in steady laminar motion in the annulus with a developing velocity profile. In the region $z < 0$, the fluid and both walls are maintained at a uniform temperature T_o. In the region $z > 0$, a constant temperature, $T_1 \neq T_o$, is prescribed at the inner wall and the outer wall is insulated. The situation is shown in Figure 17a. It is desired to find the temperature profile and the variation of the heat transfer coefficient on the inner wall with axial distance.

Subject to the limitations mentioned in an earlier section of this chapter, the equation of energy describing the problem is

$$\rho C_p \left[v_r \frac{\partial T}{\partial r} + v_z \frac{\partial T}{\partial z}\right] = k\left[\frac{1}{r}\frac{\partial}{\partial r}\left(r\frac{\partial T}{\partial r}\right)\right] \tag{10}$$

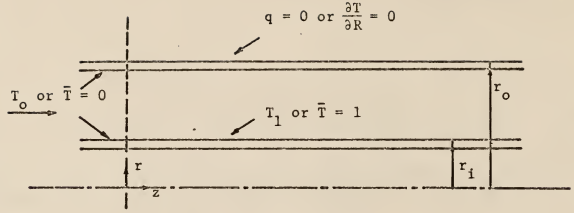

Fig. 17a. Constant temperature at the inner wall.

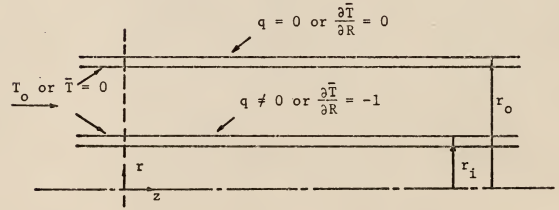

Fig. 17b. Constant heat flux at the inner wall.

with boundary conditions:

$$\begin{aligned} z \leq 0, \quad & r_i \leq r \leq r_o, \quad & T = T_o \\ z > 0, \quad & r = r_i, & T = T_1 \\ z > 0, \quad & r = r_o, & \frac{\partial T}{\partial r} = 0 \end{aligned} \tag{43}$$

As before, introducing Equation (13) and the following definition of the dimensionless temperature,

$$\bar{T} = \frac{T - T_o}{T_1 - T_o} \tag{44}$$

the energy equation in dimensionless form then becomes

$$V\frac{\partial \bar{T}}{\partial R} + U\frac{\partial \bar{T}}{\partial Z} = \frac{1}{Pr}\frac{1}{R}\frac{\partial}{\partial R}\left(R\frac{\partial \bar{T}}{\partial R}\right) \tag{45}$$

where Pr is the Prandtl number. The corresponding boundary conditions are as follows:

$$\begin{aligned} Z \leq 0, \quad & 1 \leq R \leq r_o/r_i, \quad & \bar{T} = 0 \\ Z > 0, \quad & R = 1, & \bar{T} = 1 \\ Z > 0, \quad & R = r_o/r_i, & \frac{\partial \bar{T}}{\partial R} = 0 \end{aligned} \tag{46}$$

The axial and radial velocity distributions being known, Equation (45) can be solved readily to give the temperature profile. Unlike the velocity profiles, solution of Equation (45) involves no trial and error and the procedure is straight-forward. In addition to the radius ratio r_o/r_i, the Prandtl number, Pr, appears in the energy equation. The effect of this dimensionless quantity will be discussed later.

$$C(j,k) = -\frac{\Delta R}{2}V(j,k) + \frac{\Delta R}{2R(k)Pr} - \frac{1}{Pr}$$

$$A(j,k) = \frac{2}{Pr} + \frac{(\Delta R)^2}{\Delta Z}U(j,k) \qquad (50)$$

$$B(j,k) = \frac{\Delta R}{2}V(j,k) - \frac{\Delta R}{2PrR(k)} - \frac{1}{Pr}$$

$$D(j,k) = \frac{(\Delta R)}{\Delta Z}U(j,k)\bar{T}(j,k)$$

with boundary conditions

$$\begin{aligned} &Z \leq 0, && 1 \leq R \leq r_o/r_i, && \bar{T} = 0 \\ &Z > 0, && R = 1, && \bar{T}(j+1,1) = 1 \\ &Z > 0, && R = r_o/r_i, && \bar{T}(j+1,n) = \bar{T}(j+1,n+1). \end{aligned} \qquad (51)$$

The quantities $\bar{T}(j+1,n+1)$ and $\bar{T}(j+1,n)$ represent the temperatures at the outer wall and at the point adjacent to the wall respectively.

Equations similar to Equation (49) can be written for every interior point k for a particular column j+1. Thus for k=2, Equation (49) becomes

$$C(j,2)\bar{T}(j+1,1)+A(j,2)\bar{T}(j+1,2)+B(j,2)\bar{T}(j+1,3) = D(j,2)$$

Application of the second boundary condition of Equation (51) then gives

$$A(j,2)\bar{T}(j+1,2)+B(j,2)\bar{T}(j+1,3) = D(j,2)-C(j,2) \qquad (52)$$

For k=3,4, ..., n-1, the following equations can be written

A.2. Solution of the equation.

To obtain the temperature profiles by solving the energy equation, the finite difference technique with the Thomas method used to solve the resulting algebraic equations will again be employed. The following finite difference approximations are introduced:

$$\frac{\partial \bar{T}}{\partial Z} = \frac{\bar{T}(j+1,K) - \bar{T}(j,k)}{\Delta Z}$$

$$\frac{\partial \bar{T}}{\partial R} = \frac{\bar{T}(j+1,k+1) - \bar{T}(j+1,k-1)}{2(\Delta R)} \tag{47}$$

$$\frac{\partial^2 \bar{T}}{\partial R^2} = \frac{\bar{T}(j+1,k+1) - 2\bar{T}(j+1,k) + \bar{T}(j+1,k-1)}{(\Delta R)^2}$$

Substitution of these approximations into the energy equation yields

$$V(j,k)\frac{\bar{T}(j+1,k+1)-\bar{T}(j+1,k-1)}{2(\Delta R)} + U(j,k)\frac{\bar{T}(j+1,k)-\bar{T}(j,k)}{\Delta Z}$$

$$= \frac{1}{Pr}\frac{1}{R(k)}\frac{\bar{T}(j+1,k+1)-\bar{T}(j+1,k-1)}{2(\Delta R)} + \frac{1}{Pr}\frac{\bar{T}(j+1,k+1)-2\bar{T}(j+1,k)+\bar{T}(j+1,k-1)}{(\Delta R)^2} \tag{48}$$

After rearrangement, the energy equation takes the form

$$C(j,k)\bar{T}(j+1,k-1)+A(j,k)\bar{T}(j+1,k)+B(j,k)\bar{T}(j+1,k+1)=D(j,k) \tag{49}$$

where

$$C(j,3)T(j+1,2)+A(j,3)\bar{T}(j+1,3)+B(j,3)\bar{T}(j+1,4) = D(j,3)$$

$$C(j,n-1)\bar{T}(j+1,n-2)+A(j,n-1)\bar{T}(j+1,n-1)+B(j,n-1)\bar{T}(j+1,n) = D(j,n-1)$$

For k=n, again, some rearrangement is necessary.

$$C(j,n)\bar{T}(j+1,n-1)+A(j,n)\bar{T}(j+1,n)+B(j,n)\bar{T}(j+1,n+1)=D(j,n)$$

According to the third condition of Equation (51), it can be rewritten as

$$C(j,n)\bar{T}(j+1,n-1)+[A(j,n)+B(j,n)]\bar{T}(j+1,n)=D(j,n) \qquad (54)$$

Equations (52), (53) and (54) then constitute a set of n-1 linear algebraic equations with the same number of unknowns. They can be solved by the Thomas method without difficulty. The procedure is much the same as in solving the momentum and continuity equations for the velocity profile except in this case it is simpler because no trial and error is involved. Sample results are shown graphically in Figures 18 and 19.

The problem of discontinuity at the points k=1, j=1 and k=n+1, j=1 does not exist in solving the energy equation. Examination of Equations (52), (53) and (54) shows that no information on the values of $\bar{T}(1,1)$ and $\bar{T}(1,n+1)$ is needed to start the calculation. The Thomas method is applied at each column and the values of the radial and axial velocities are directly employed in these equations. Calculations can proceed in this manner until the temperature profile no longer changes with axial distance.

A.3. The bulk temperature and the Nusselt number.

The determination of the variation of the Nusselt number on the inner surface along the length of the annulus is the main purpose of this work.

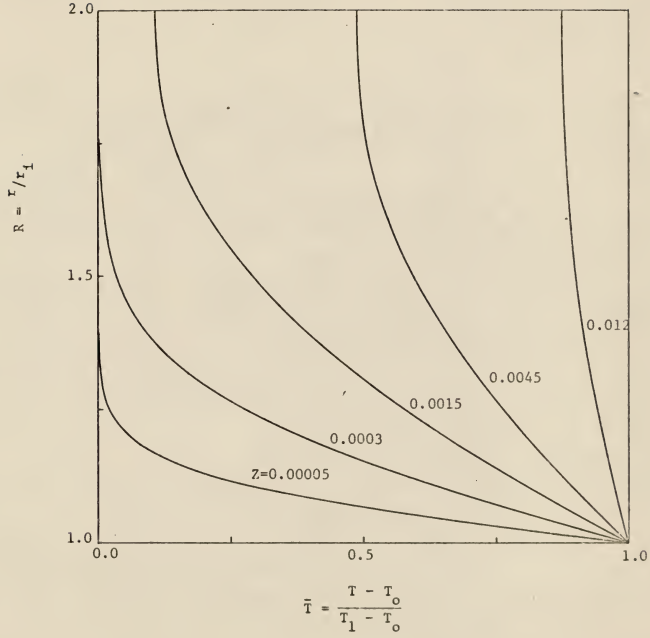

Fig. 18. Developing temperature profiles for Case I, $r_o/r_i = 2.0$ and $P_r = 0.01$.

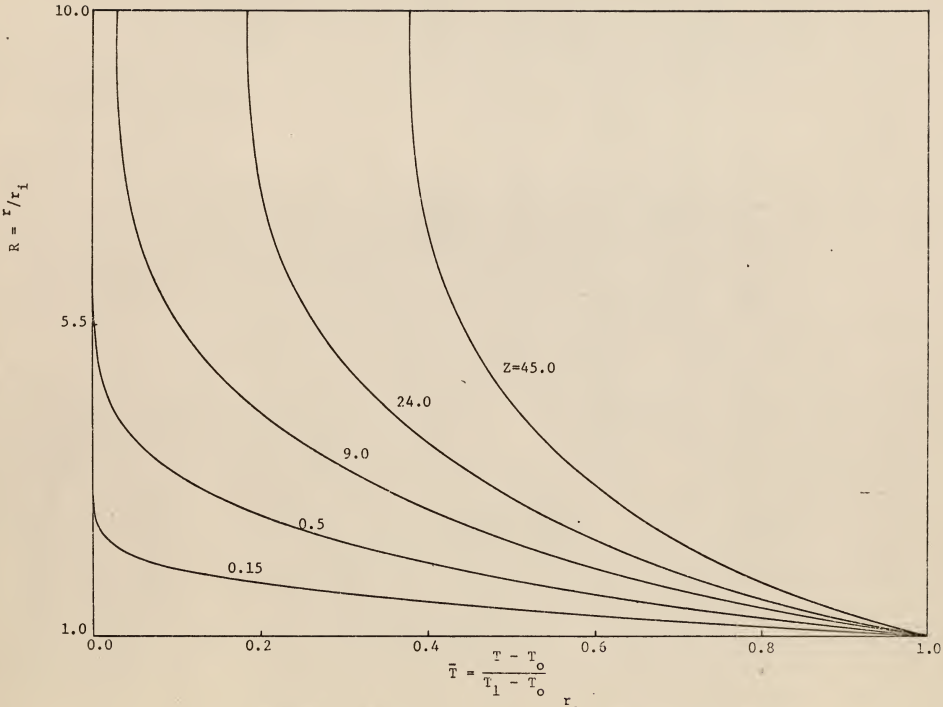

Fig. 19. Developing temperature profiles for Case I, $r_o/r_i = 10.0$ and $P_r = 1.0$.

But before the expression for the Nusselt number can be derived, the mixing-cup or bulk temperature, T_b, must first be determined. By definition,

$$T_b = \frac{\int_0^{2\pi}\int_{r_i}^{r_o} v_z T r d\theta dr}{\int_0^{2\pi}\int_{r_i}^{r_o} v_z r d\theta dr} \tag{55}$$

Introduction of the dimensionless quantities defined in Equations (13) and (44) gives

$$\bar{T}_b = \frac{\int_0^{2\pi}\int_1^{r_o/r_i} U\bar{T} R d\theta dR}{\int_0^{2\pi}\int_1^{r_o/r_i} U R d\theta dR}$$

$$= \frac{2}{\left[\left(\frac{r_o}{r_i}\right)^2 - 1\right]} \int_1^{r_o/r_i} U\bar{T} R dR \,, \tag{56}$$

The integral in Equation (56) can be evaluated numerically with the known velocity and temperature profiles. Thus for column j+1, application of the trapezoidal rule leads to

$$\bar{T}_b = \frac{2\Delta R}{\left[\left(\frac{r_o}{r_i}\right)^2 - 1\right]} \sum_{k=2}^{n} U(j+1,k)\bar{T}(j+1,k)R(k) \tag{57}$$

in which U vanishes at k=1 and k=n+1.

The Nusselt number is defined by

$$Nu_i = \frac{h_i D_e}{k} \tag{58}$$

The equivalent diameter D_e and the heat transfer coefficient are defined by the following equations:

$$D_e = 2(r_o - r_i)$$

$$= 2r_i\left(\frac{r_o}{r_i} - 1\right) \tag{59}$$

$$h_i(T_w - T_b) = -k\left(\frac{\partial T}{\partial r}\right)_{r = r_i} \tag{60}$$

Therefore, the Nusselt number on the inner surface is

$$Nu_i = \frac{-k\left(\frac{\partial T}{\partial r}\right)_{r=r_i}}{T_w - T_b} \cdot \frac{2r_i\left(\frac{r_o}{r_i} - 1\right)}{k}$$

$$= -2\left(\frac{r_o}{r_i} - 1\right)\frac{\left(\frac{\partial \bar{T}}{\partial R}\right)_{R=1}}{1 - \bar{T}_b} \tag{61}$$

where the fact that the dimensionless inner wall temperature is unity has been utilized.

To evaluate the temperature gradient at the inner wall, the following reasoning is adopted. At the inner wall, the dimensionless equation of energy, Equation (45), may be written as

$$0 = \frac{\partial}{\partial R}\left(R\frac{\partial \bar{T}}{\partial R}\right)$$

$$= \frac{\partial \bar{T}}{\partial R} + R\frac{\partial^2 \bar{T}}{\partial R^2}$$

or

$$\frac{1}{R}\frac{\partial \bar{T}}{\partial R} + \frac{\partial^2 \bar{T}}{\partial R^2} = 0 \tag{62}$$

Substituting Equation (47) into the above equation, the following difference equation is obtained for column j+1.

$$\frac{1}{R(1)}\frac{\bar{T}(j+1,2)-\bar{T}(j+1,0)}{2\Delta R} + \frac{\bar{T}(j+1,2)-2\bar{T}(j+1,1)+\bar{T}(j+1,0)}{(\Delta R)^2} = 0. \tag{63}$$

$\bar{T}(j+1,0)$ is the temperature of a hypothetical point inside the wall as shown in the sketch.

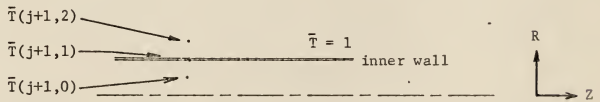

Rearrangement of Equation (63) gives $\bar{T}(j+1,0)$ in terms of $\bar{T}(j+1,2)$ and $\bar{T}(j+1,1)$.

Thus,

$$\bar{T}(j+1,0) = \frac{\frac{2}{(\Delta R)^2}\bar{T}(j+1,1) - [\frac{1}{2R(1)\Delta R} + \frac{1}{(\Delta R)^2}]\bar{T}(j+1,2)}{\frac{1}{(\Delta R)^2} - \frac{1}{2R(1)\Delta R}}$$

$$= \frac{2\bar{T}(j+1,1) - (\frac{\Delta R}{2+1})\bar{T}(j+1,2)}{1 - \frac{\Delta R}{2}} \tag{64}$$

since R(1)=1.

The temperature gradient at the inner wall is then

$$\left(\frac{\partial \bar{T}}{\partial R}\right)_{R=1} = \frac{\bar{T}(j+1,2)-\bar{T}(j+1,0)}{2(\Delta R)}$$

$$= \frac{1}{2(\Delta R)}\left[\bar{T}(j+1,2) - \frac{2\bar{T}(j+1,1)-\left(\frac{\Delta R}{2}+1\right)\bar{T}(j+1,2)}{1-\frac{\Delta R}{2}}\right]$$

$$= \frac{\bar{T}(j+1,2)-\bar{T}(j+1,1)}{\Delta R\left(1-\frac{\Delta R}{2}\right)} \tag{65}$$

Substitution of this result into Equation (61) gives finally

$$Nu_i = 2\left(\frac{r_o}{r_i} - 1\right)\frac{\bar{T}(j+1,1)-\bar{T}(j+1,2)}{\Delta R(1-\bar{T}_b)\left(1-\frac{\Delta R}{2}\right)} \tag{66}$$

The variation of the Nusselt number with the axial distance is plotted in Figures 20 and 21. Values of 0.01, 1.0 and 10.0 have been considered for the Prandtl number.

B. Case II: Constant heat flux at the inner wall and outer wall insulated.

B.1. Statement and solution of the problem.

The flow conditions for the constant flux case are the same as in the previous section, but the boundary condition on the inner surface is different. Instead of maintaining the inner wall at constant temperature, a uniform heat flux is prescribed on it as shown in Figure 17b. The boundary conditions are as follows:

$$\begin{aligned} &z \leq 0, && r_i \leq r \leq r_o, && T = T_o \\ &z > 0, && r = r_i, && -k\frac{\partial T}{\partial r} = q \\ &z > 0, && r = r_o, && \frac{\partial T}{\partial r} = 0 \end{aligned} \tag{67}$$

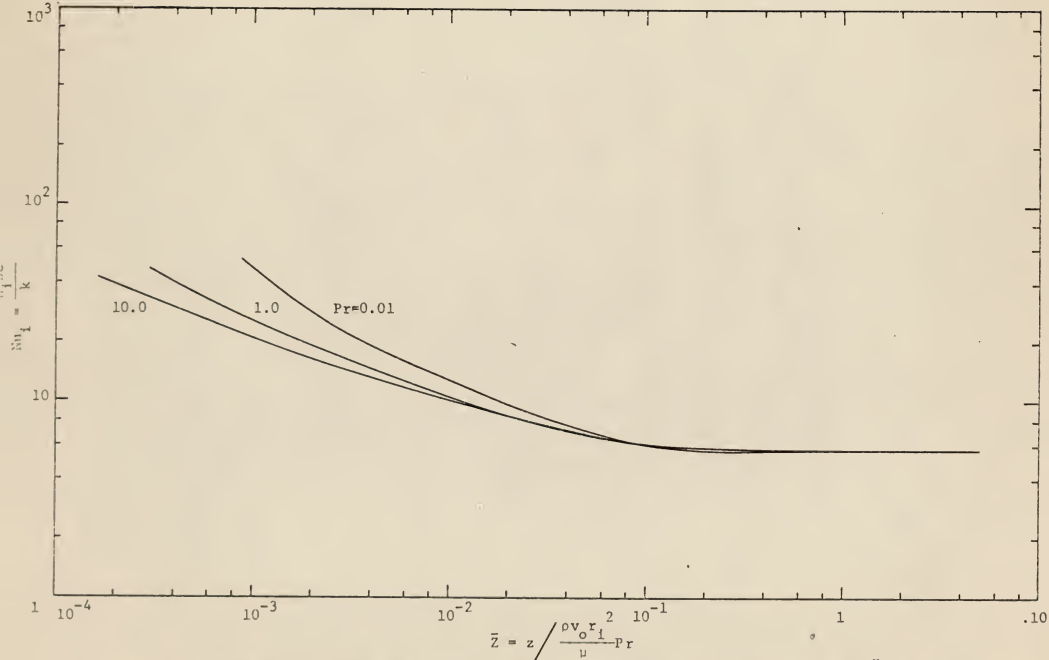

Fig. 20. Variation of Nusselt number with axial distance for various Prandtl number, $\frac{r_o}{r_i} = 2.0$, Case I.

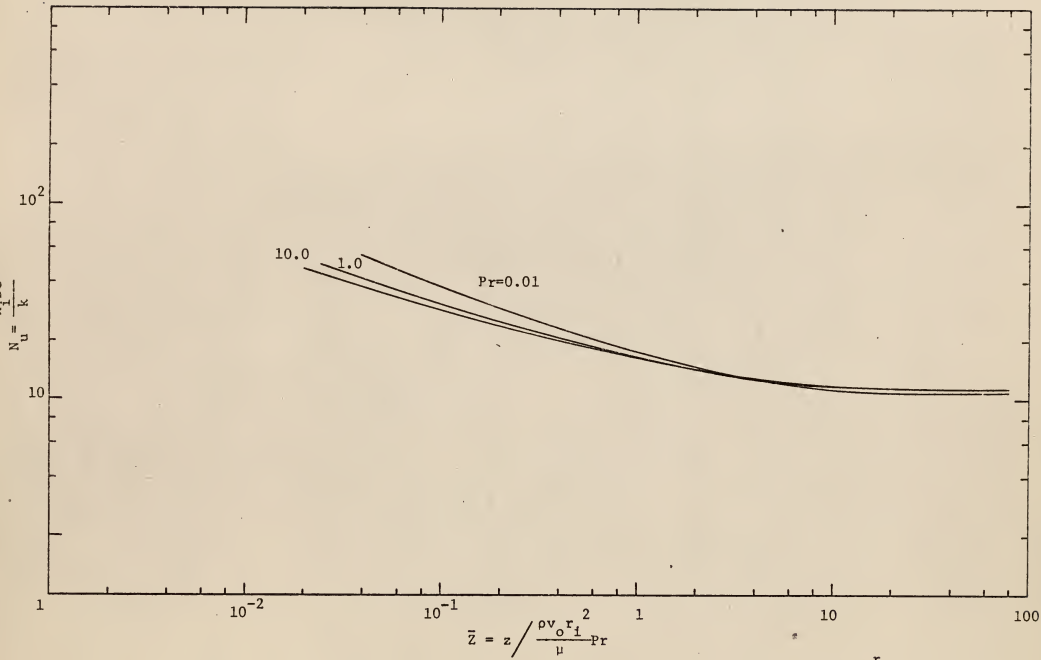

Fig. 21. Variation of Nusselt number with axial distance for various Prandtl numbers, r_o/r_i = 10.0, Case I.

A convenient form for the dimensionless temperature in this case is,

$$T = \frac{T - T_o}{qr_i/k} , \tag{68}$$

where q is the constant heat flux prescribed at the inner wall. The energy equation, in dimensionless form, then becomes

$$V\frac{\partial \bar{T}}{\partial R} + U\frac{\partial \bar{T}}{\partial Z} = \frac{1}{Pr}[\frac{1}{R}\frac{}{R}(R\frac{\partial \bar{T}}{\partial R})] \tag{45}$$

and the corresponding boundary conditions are

$$\begin{array}{lll} Z \leq 0, & 1 \leq R \leq r_o/r_i, & \bar{T} = 0 \\ Z > 0, & R = 1, & \frac{\partial \bar{T}}{\partial R} = -1 \\ Z > 0, & R = r_o/r_i, & \frac{\partial \bar{T}}{\partial R} = 0. \end{array} \tag{69}$$

Introduction of the difference quotients in Equation (47) reduces the energy equation to equations exactly the same as (49) and (50). At the inner wall, combination of Equation (65) and the second condition of (69) yields

$$(\frac{\partial \bar{T}}{\partial R})_{R=1} = \frac{\bar{T}(j+1,2)-\bar{T}(j+1,1)}{R(1 - \frac{\Delta R}{2})}$$

$$= -1$$

or

$$\bar{T}(j+1,1) = \bar{T}(j+1,2) + \Delta R(1 - \frac{\Delta R}{2}) \tag{70}$$

and at the outer wall,

$$\frac{\partial \bar{T}}{\partial R} = \frac{\bar{T}(j+1,n)-\bar{T}(j+1,n+1)}{\Delta R}$$

or

$$\bar{T}(j+1,n) = \bar{T}(j+1,n+1) \tag{71}$$

Therefore, for column j+1, the following equations can be written for k=2, 3, ..., n:

$$\begin{aligned}
&[C(j,2)+A(j,2)]\bar{T}(j+1,2)+B(j,2)\bar{T}(j+1,3)=D(j,2)-C(j,2)\Delta R(1-\frac{\Delta R}{2})\\
&C(j,3)\bar{T}(j+1,2)+A(j,3)\bar{T}(j+1,3)+B(j,3)\bar{T}(j+1,4)+D(j,3)\\
&\text{----------}\\
&\text{----------}\\
&C(j,n)\bar{T}(j+1,n-1)+[A(j,n)B(j,n)]\bar{T}(j+1,n)=D(j,n)
\end{aligned} \tag{72}$$

These linear algebraic equations have been solved by the Thomas method on a digital computer and the temperature profiles are shown in Figures 22 and 23 for r_o/r_i=2.0 and 10.0 and Pr=0.01, 1.0.

B.2. The bulk temperature and the Nusselt number

Once the temperature distribution is known, the bulk temperature can be evaluated numerically from Equation (57). However, for the case of uniform heat flux prescribed at the inner wall, a simple relation exists between the bulk temperature and the axial distance from the inlet. The derivation is as follows:

An energy balance is made between the entrance and an arbitrary distance z downstream. The resulting equation is

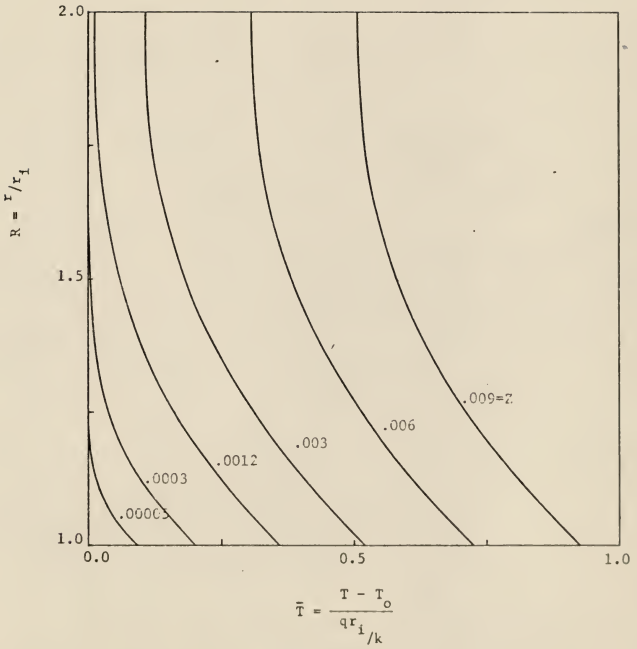

Fig. 22. Developing temperature profiles for Case II, $r_o/r_i = 2.0$ and Pr = 0.01.

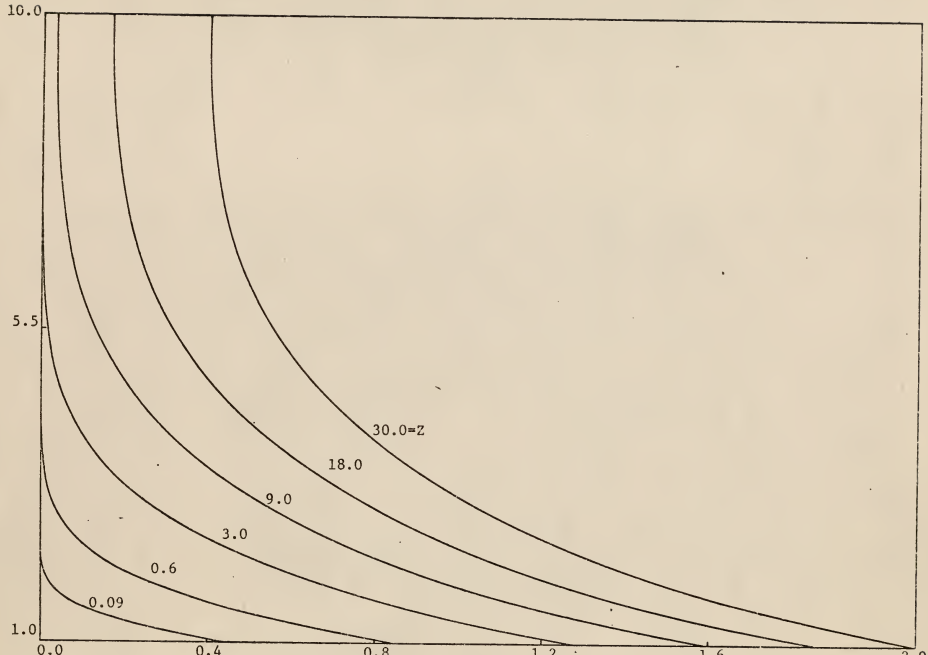

Fig. 23. Developing temperature profiles for Case II, $r_o/r_i = 10.0$ and Pr = 1.0.

$$(2\pi r_i z)q = \int_0^{2\pi} \int_{r_i}^{r_o} C_p(T-T_o)v_z r d\theta dr \tag{73}$$

which states that the heat entering through the walls is the same as the difference between the heat transported through the cross section at z=0 and z=z. T_o is a reference temperature and in this case it is the entering fluid temperature. By introducing the corresponding dimensionless variables, Equation (73) becomes

$$\frac{2\pi Z}{Pr} = \int_0^{2\pi} \int_1^{r_o/r_i} U\bar{T}R d\theta dR$$

or

$$\frac{Z}{Pr} = \int_1^{r_o/r_i} U\bar{T}R dR \tag{74}$$

Substitution of Equation (56) into the above equation then yields the desired relation. Thus,

$$\frac{Z}{Pr} = \frac{1}{2}\bar{T}_b\left[\left(\frac{r_o}{r_i}\right)^2 - 1\right]$$

$$\bar{T}_b = \frac{2Z}{Pr\left[\left(\frac{r_o}{r_i}\right)^2 - 1\right]} \tag{75}$$

The bulk temperature at any arbitrary distance from the inlet can then be evaluated readily from Equation (75) without knowing the temperature distribution across the annular space at that particular distance.

The Nusselt number, in terms of dimensionless variables for this

problem becomes

$$Nu_i = 2\left(\frac{r_o}{r_i} - 1\right)\frac{-\left(\frac{\partial \bar{T}}{\partial R}\right)R = 1}{\bar{T}_w - \bar{T}_b}$$

$$= 2\left(\frac{r_o}{r_i} - 1\right)\frac{1}{\bar{T}_w - \bar{T}_b} \qquad (76)$$

where $\bar{T}_w$ is the inner wall temperature and is equal to $\bar{T}(j+1,1)$.

The bulk temperature and Nusselt number are plotted versus the axial distance for $\frac{r_o}{r_i}$ = 2.0 and 10.0 and Pr = 0.01, 1 and 10 respectively in Figures 24 and 25.

It is of interest to note that the bulk temperatures for the uniform heat flux case calculated from Equations (75) and (57) differ by as much as 10% at regions very close to the inlet.

C. Results and Discussion

The developing temperature profile in the entrance region of an annulus has been obtained for two boundary conditions on the inner surfaces, namely (i) constant temperature and (ii) constant heat flux. In both cases the outer surface is insulated. Sample results are shown graphically in Figures 18, 19, 22 and 23 since it is not practical to give temperature distribution as a function of axial distance for all values of the radius ratio and the Prandtl number.

The mesh sizes for the energy equation are tabulated in Tables 4 and 5. Due to the fact that the variation of the velocity in the vicinity of the inlet is large, very small increments in the axial direction were used in the momentum and continuity equations. These were gradually increased along the annulus until a final value of 1/20 was reached when the velocity profile

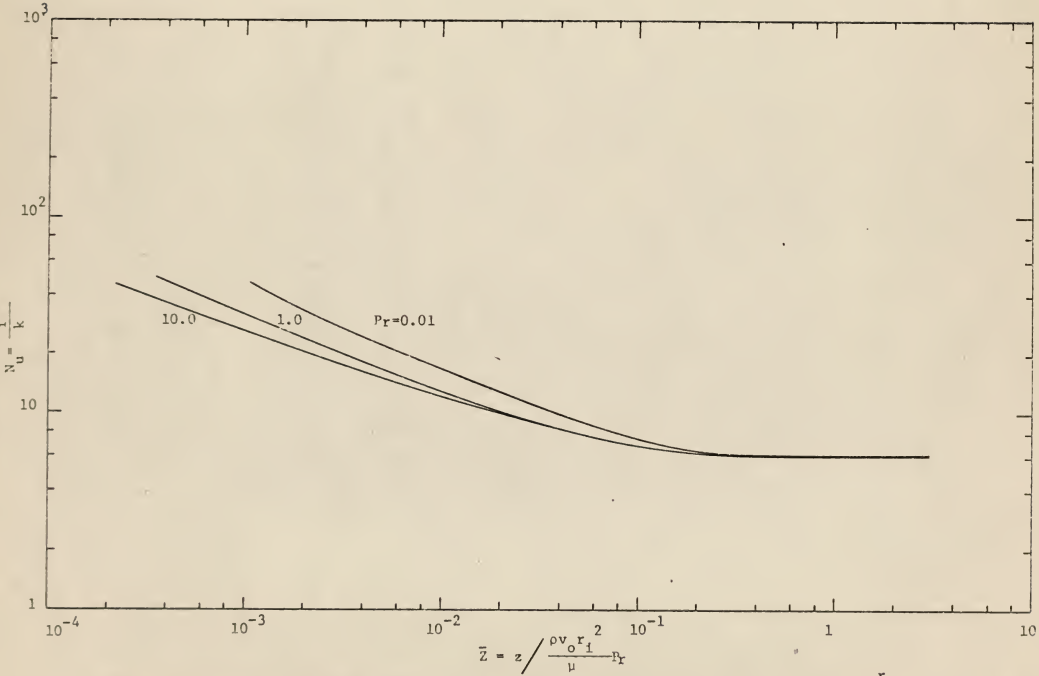

Fig. 24. Variation of Nusselt number with axial distance for various Prandtl numbers, $\frac{r_o}{r_i} = 2.0$, Case II.

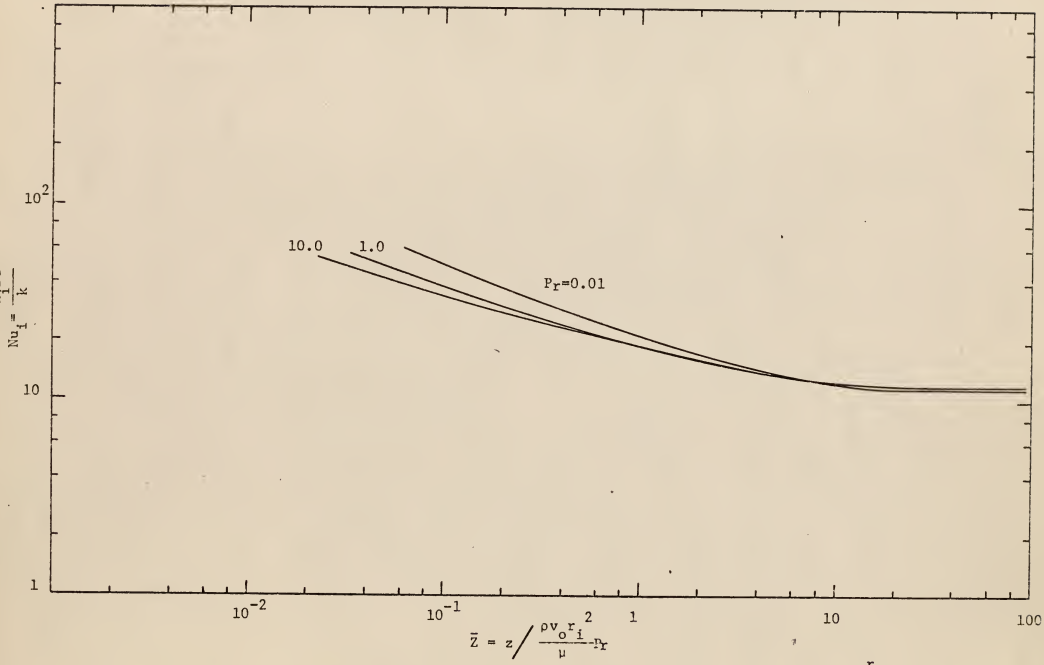

Fig. 25. Variation of Nusselt number with axial distance for various Prandtl numbers, r_o/r_i = 10.0, Case II.

Table 4. Mesh sizes for the energy equation, Pr = 0.01.

Radius ratio r_o/r_i	Mesh number of R	Z	ΔZ	ΔR
		0.0		
2.0	51		0.00001	0.02
		0.0015		
			0.00005	0.02
		fully-developed		
		0.0		
10.0	151		0.00001	0.06
		0.0003		
			0.00005	0.06
		0.0024		
			0.0001	0.06
		0.009		
			0.0002	0.06
		0.045		
			0.0005	0.06
		0.108		
			0.001	0.06
		0.24		
			0.002	0.06
		fully-developed		

Table 5. Mesh sizes for the energy equation, Pr = 1.0 and 10.0.

Radius ratio r_o/r_i	Mesh number of R	Z	ΔZ	ΔR
2.0	51	0.0		
		0.0015	0.00006	0.02
		0.0108	0.0003	0.02
		0.0906	0.0006	0.02
		0.4206	0.003	0.02
		1.0206	0.006	0.02
		10.0	0.03	0.02
10.0	151	0.0		
		0.0003	0.00006	0.06
		0.0024	0.0003	0.06
		0.009	0.0006	0.06
		0.045	0.0012	0.06
		0.108	0.003	0.06
		0.3	0.006	0.06
		1.14	0.012	0.06
		3.0	0.03	0.06
		7.8	0.06	0.06
		15.6	0.12	0.06
		51.0	0.3	0.06
		92.0	0.5	0.06
		380.0	1.0	0.06

became fully developed. For the energy equation, however, increments as large as six times the ones used for the momentum and continuity equations were employed. Since the temperature distribution was determined from the known velocity profile, it is believed that a larger axial increment for the energy equation will not lead to significant error.

The surface and bulk temperature variation for various radius ratios and Prandtl numbers are shown in Figures 26-29. It can be seen that the surface (for the constant flux case) and bulk temperatures increase very sharply for small Prandtl numbers, say 0.01, and very slowly for large Prandtl numbers such as 10.0. For the case of constant heat flux at the inner wall, the bulk temperature is a linear function of axial distance as defined by Equation (75). The large difference between the surface and bulk temperatures for a radius ratio of 10.0 is expected as the thermal boundary layer extends over such a small fraction of the cross section in the entrance region.

The variation of the Nusselt numbers with axial distance are presented in Figures 20, 21, 24 and 25. A convenient form of the axial distance defined as $\bar{Z} = Z/Pr$ has been used. Results of the asymptotic Nusselt number are also presented in Table 6, along with analytical results obtained by Lundberg et al. (10). The maximum deviation is shown to be less than 5 per cent with the largest deviation occurring when the Prandtl number is 0.01. This trend was expected since for fluids with very low Prandtl number, the temperature profile is established much faster than the velocity profile and slight error in the velocity distribution might lead to significant error in the temperature profile. In contrast, for large Prandtl numbers, the velocity profile develops more rapidly and more accurate temperature profiles

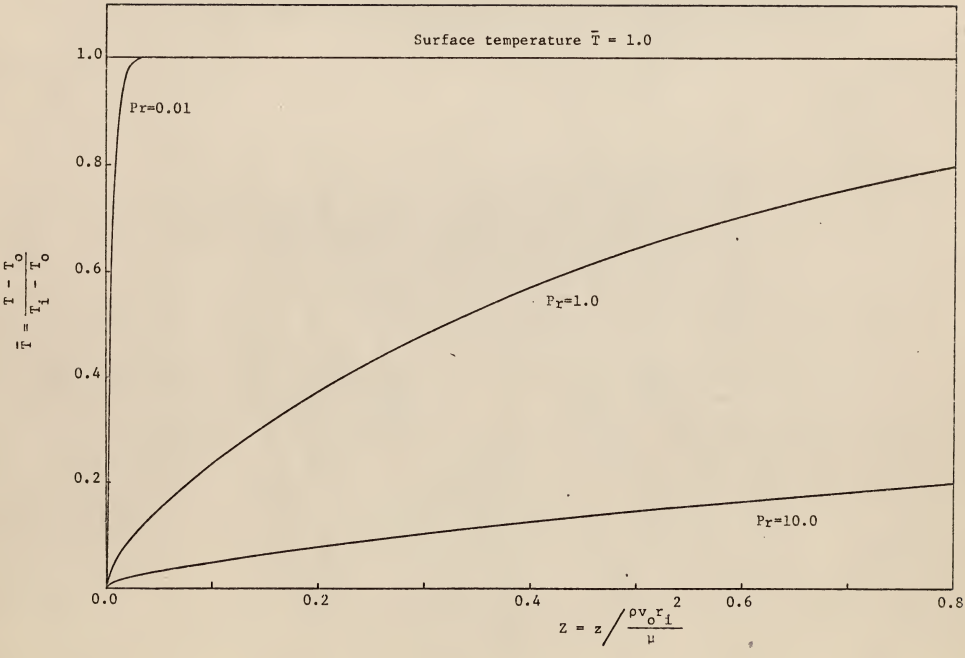

Fig. 26. Bulk and surface temperature variations for various Prandtl number in the entrance region, $\frac{r_o}{r_i}$ = 2.0, Case I.

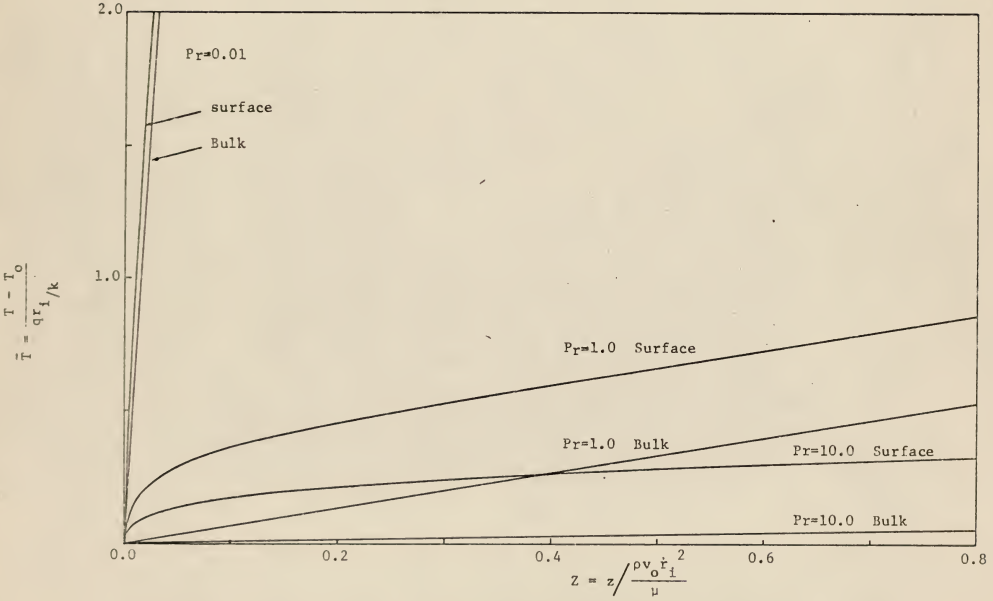

Fig. 27. Bulk and surface temperature variation for various Prandtl number in the entrance region, $\frac{r_o}{r_i} = 2.0$, Case II.

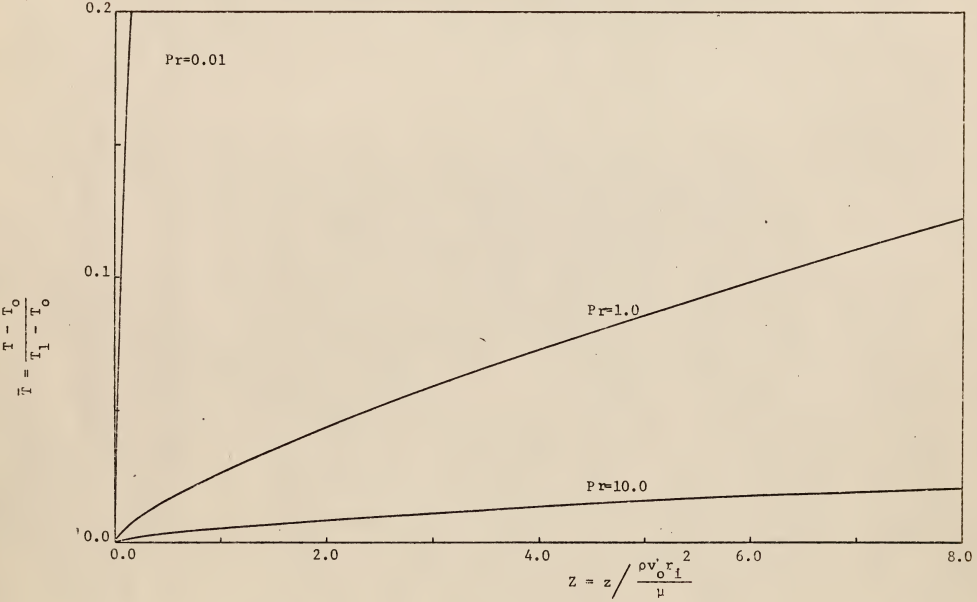

Fig. 28. Bulk temperature variations for various Prandtl numbers in the entrance region, $r_o/r_i = 10.0$, Case I.

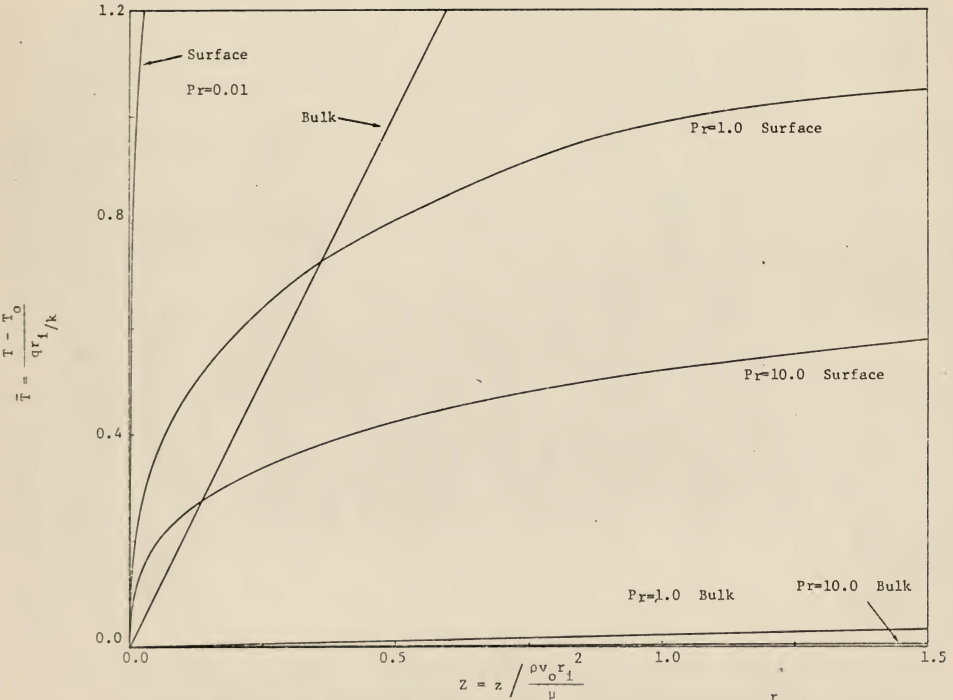

Fig. 29. Bulk and surface temperature variation for various Prandtl numbers, $\frac{r_o}{r_1} = 10.0$, Case II.

Table 6. Comparison of analytical and numerical asymptotic values of the Nusselt number.

Case I: Constant temperature at the inner wall and outer wall insulated.

Radius ratio r_o/r_i	Prandtl number Pr	Asymptotic Nu_i Analytical	Numerical	% error
2.0	0.01	5.738	5.73	0.14
	1.0	5.738	5.738	0.0
	10.0	5.738	5.742	0.07
10.0	0.01	11.56	11.07	4.24
	1.0	11.56	11.574	0.12
	10.0	11.56	11.587	0.23

Case II: Constant heat flux at the inner wall and outer wall insulated.

2.0	0.01	6.181	6.145	0.58
	1.0	6.181	6.085	1.54
	10.0	6.181	6.189	0.13
10.0	0.01	11.90	11.511	3.27
	1.0	11.90	11.94	0.34
	10.0	11.90	11.984	0.71

could be obtained. Both the velocity and temperature distribution develop at an approximately similar rate for Prandtl numbers near unity. There are fluctuations in the values of the Nusselt number near the entrance. However, they smooth down quickly as the profile develops.

Several attempts have been made to improve the calculated Nusselt number. By means of a linear interpolation, the velocity profile for a mesh with size double the original one could be obtained. The temperature profile and thus the Nusselt number were then calculated using the new velocity profile. A better approximation (21) to the temperature gradient at the inner wall has also been attempted. The gradient can be written as

$$\frac{\partial \bar{T}}{\partial R} = \frac{1}{2(\Delta R)}[4\bar{T}(R+\Delta R) - 3\bar{T}(R) - \bar{T}(R+2\Delta R)] \tag{77}$$

where $\bar{T}(R)$ represents the temperature at the wall and $\bar{T}(R+\Delta R)$ and $\bar{T}(R+2\Delta R)$ represent the temperatures at two consecutive points out from the wall. The situation is shown in the sketch.

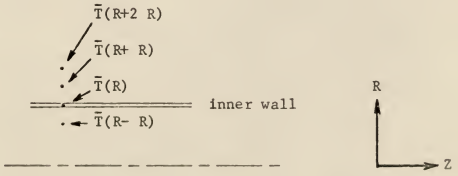

Equation (77) can be written in terms of the subscript notation as

$$\frac{\partial \bar{T}}{\partial R} = \frac{1}{2(\Delta R)}[4\bar{T}(j+1,2) - 3\bar{T}(j+1,1) - \bar{T}(j+1,3)] \tag{78}$$

The Nusselt number for the case of constant wall temperature then becomes

$$Nu_i = \left(\frac{r_o}{r_i} - 1\right)\frac{1}{\Delta R}[4\bar{T}(j+1,2) - 3\bar{T}(j+1,1) - \bar{T}(j+1,3)] \tag{79}$$

where the wall temperature $\bar{T}(j+1,1)$ is unity.

For the case of constant heat flux at the inner wall, application of the second boundary condition of Equation (69) yields

$$\left(\frac{\partial \bar{T}}{\partial R}\right)_{R=1} = \frac{1}{2(\Delta R)}[4\bar{T}(j+1,2) - 3\bar{T}(j+1,1) - \bar{T}(j+1,3)] = -1$$

or

$$\bar{T}(j+1,1) = \frac{1}{3}[2\Delta R + 4\bar{T}(j+1,2) - \bar{T}(j+1,3)] \tag{80}$$

The Nusselt number is then

$$Nu_i = 2\left(\frac{r_o}{r_i} - 1\right)\frac{1}{\bar{T}(j+1,1) - \bar{T}_b} \tag{81}$$

Had the temperature of a hypothetical point inside the wall been taken into consideration in place of $\bar{T}(R+2\Delta R)$, a different form of the temperature gradient would have resulted, i.e.,

$$\frac{\partial \bar{T}}{\partial R} = \frac{1}{2\Delta R}[4\bar{T}(j+1,1) - 3\bar{T}(j+1,0) - \bar{T}(j+1,2)] \tag{82}$$

Substitution of Equation (64) into the above equation gives, after rearrangement,

$$\frac{\partial \bar{T}}{\partial R} = \frac{(1+\Delta R)\ [\bar{T}(j+1,2) - \bar{T}(j+1,1)]}{R(1 - \frac{\Delta R}{2})} \tag{83}$$

The wall temperature and the Nusselt numbers can be calculated with some

manipulation.

Case I:

$$Nu_i = 2\left(\frac{r_o}{r_i} - 1\right) \frac{(1+\Delta R)\ [\bar{T}(j+1,1) - \bar{T}(j+1,2)]}{R(1 - \bar{T}_b)(1 - \frac{\Delta R}{2})} \tag{84}$$

Case II:

$$\bar{T}(j+1,1) = \bar{T}(j+1,2) + \frac{R(1 - \frac{\Delta R}{2})}{(1+\Delta R)} \tag{85}$$

$$Nu_i = 2\left(\frac{r_o}{r_i} - 1\right) \frac{1}{\bar{T}(j+1,1) - \bar{T}_b} \tag{86}$$

Table 7 shows a comparison of the wall temperatures and Nusselt numbers obtained by these methods. It can be seen that all this rearrangement does not seem to provide improvement at all.

The Nusselt numbers obtained are compared with the analysis made by Reynolds et al. (7) in Figures 30-32. The general agreement can be considered to be reasonably good and indicates that their approximate technique is quite accurate.

Table 7. Comparison of surface temperature and Nusselt number obtained from three distinct difference equations, $r_o/r_i = 10.0$ and $Pr = 0.01$.

	Z	Surface temperature Case II	Nusselt number Nu_i Case I	Case II
	0.24	2.046490	11.0901	11.5263
#	0.24	2.046620	11.0535	11.5254
+	0.24	2.043195	11.7819	11.5507
	0.228	2.021716	11.0455	11.5302
#	0.228	2.021843	11.0092	11.5293
+	0.228	2.018422	11.7255	11.5546
	0.222	2.008661	11.0619	11.5372
#	0.222	2.008792	11.0252	11.5362
+	0.222	2.005367	11.7257	11.5616

The asymptotic Nusselt numbers are 11.56 for Case I and 11.90 for Case II.

\# values calculated from Equations (79), (80) and (81).

\+ values calculated from Equations (84), (85) and (86).

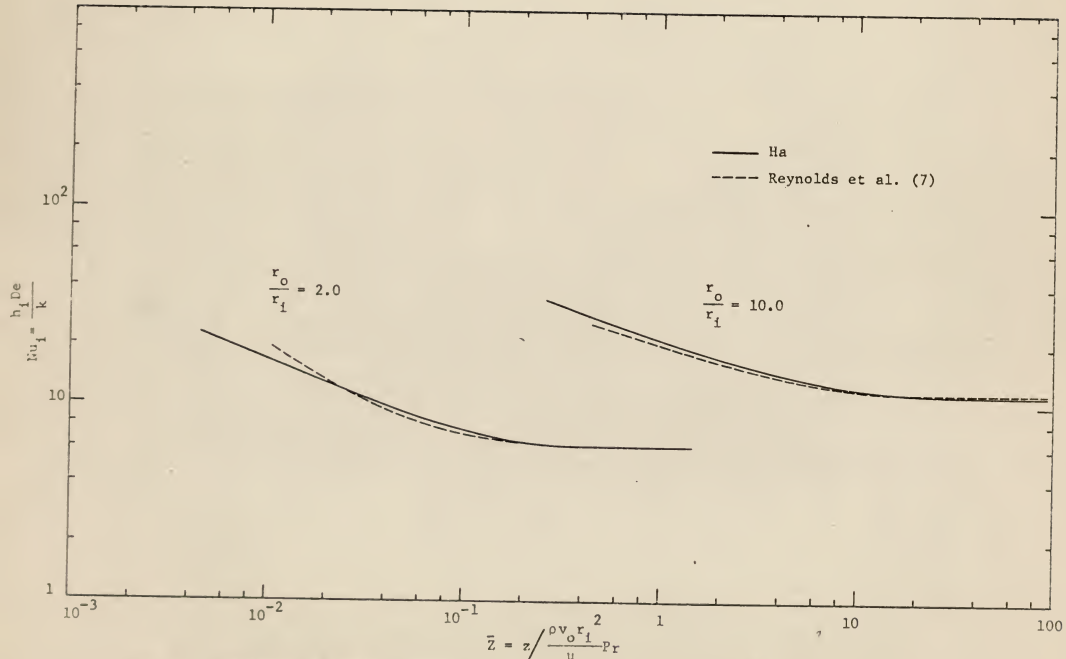

Fig. 30. Comparison of Nusselt numbers along the annulus, Case II, Pr = 0.01.

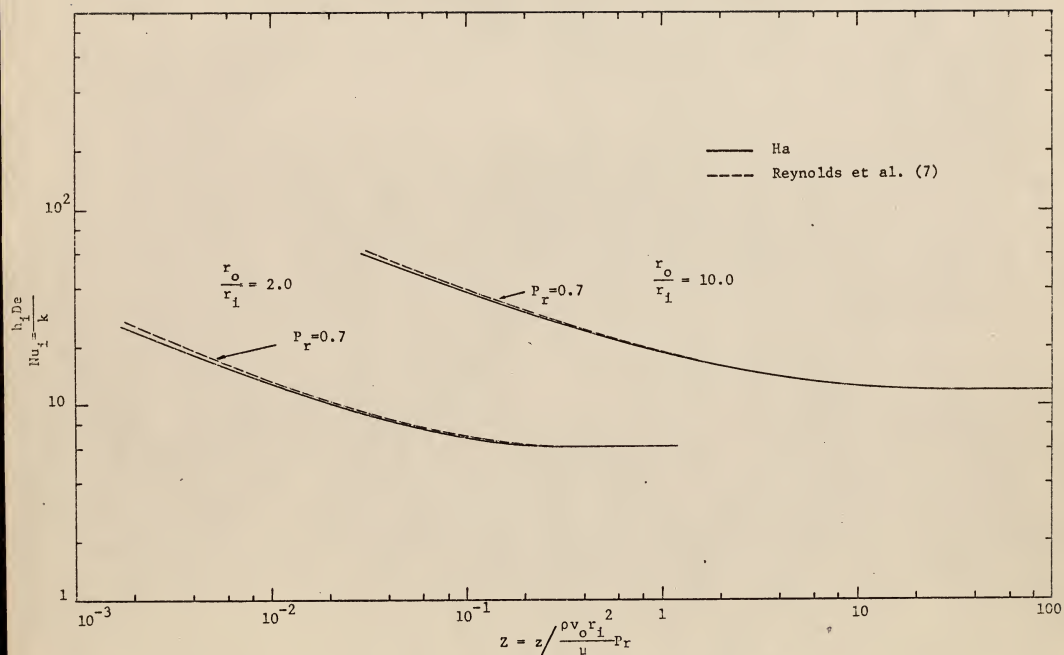

Fig. 31. Comparison of Nusselt numbers along the annulus, Case II, Pr = 1.0.

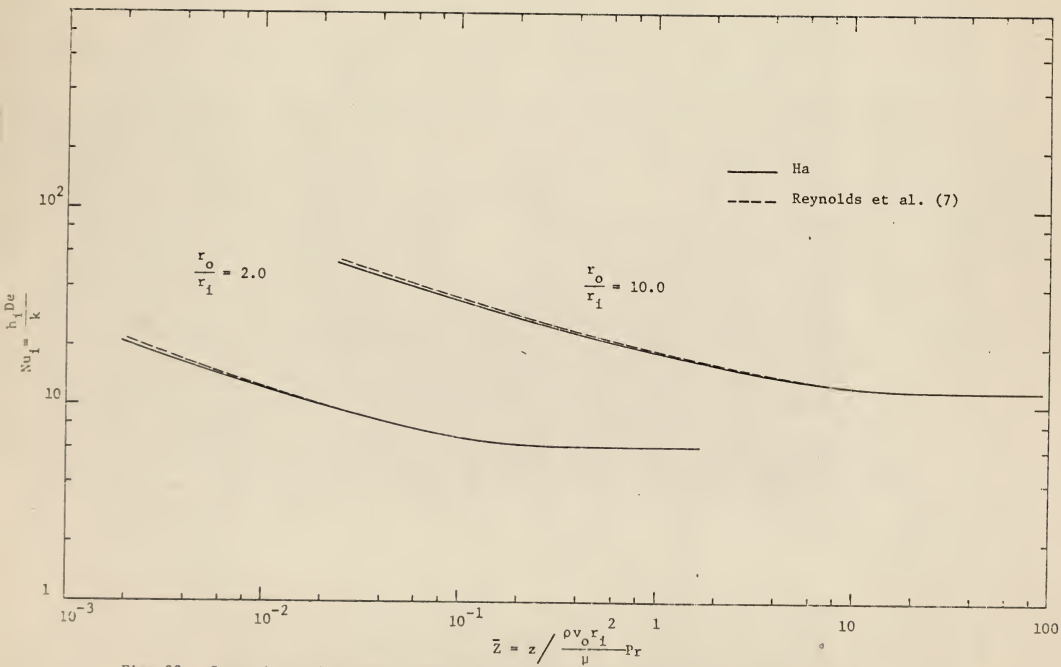

Fig. 32. Comparison of Nusselt numbers along the annulus, Case II, $Pr = 10.0$.

CHAPTER IV

SUMMARY

The problem of simultaneous development of velocity and temperature profiles in the entrance region of an annulus has been solved by the use of a numerical procedure. The system consists of highly nonlinear partial differential equations which cannot be solved otherwise. The work is applicable to all sorts of similar problems whereas approximate methods, such as Targ's linearization technique, are limited to only certain cases. For example, it would be a relatively simple task to allow for different boundary conditions or to include temperature-dependence of density and viscosity.

All papers pertinent to the work have been discussed in Chapter II. They were divided into three categories, namely (i) the velocity profile, (ii) the temperature profile and (iii) the simultaneously developing velocity and temperature profiles. Most of the investigators had employed either Targ's linearization method or Langhaar's approximation technique to linearize the momentum equation and obtained analytical solutions to the problem in terms of modified Bessel's functions. Unlike the others, Manohar (9) solved the problem numerically by an implicit finite-difference method. His results, however, were in error because of the erroneous way he treated the entrance conditions.

The momentum and continuity equations were first solved simultaneously to give the developing velocity profile and the pressure gradient. Application of the finite-difference technique reduced the problem to a set of linear algebraic equations which were solved by the Thomas method through a trial and error procedure. To render the problem soluble, a third equation,

the mass balance, was introduced as a constraint equation. Results obtained were presented graphically in Chapter III and extensive comparisons made with available data. The fully-developed velocity profile was compared with analytical results in Table 2 and agreement was excellent. The developing velocity profiles obtained by Manohar (9) were in error for both values of the radius ratio. While agreement between Sparrow and Lin's results (4) and that of this work was reasonably good for $r_o/r_i = 10.0$, Chang and Atabek's profiles (2) deviated in the vicinity of the inlet. The pressure drop results of Manohar were likewise erroneous due to the inaccuracy of his velocity profile. On the other hand, Sugino's results in the vicinity of the entrance for $r_o/r_i = 2.0$ seemed to agree with this work. A comparison of the entrance lengths in Figure 16 showed that the results obtained by Roy (3) and Chang and Atabek (2) were almost identical whereas the results of Manohar (9), Reynolds et al. (7) and this work were approximately the same. Sugino (6) concluded in his work that the entrance length was unaffected by the radius ratio r_o/r_i. Based on the calculations of this and other work, his conclusion is in error.

The values of the velocity profiles obtained were substituted into the energy equation to solve for the temperature profile. Two distinct cases with various Prandtl numbers and radius ratios were considered:

(i) Constant temperature at the inner wall, outer wall insulated,

(ii) Constant heat flux at the inner wall, outer wall insulated.

Results of the profiles as well as the bulk temperature and Nusselt number are shown graphically in Chapter III. Comparisons were made with results obtained by Reynolds et al. (7) for the constant heat flux case for $r_o/r_i = 2.0$ and 10.0 and Pr = 0.01, 1.0 and 10.0. It was concluded that

the approximate technique used by Reynolds yielded quite satisfactory heat transfer rates.

NOMENCLATURE

Symbols

C_v, C_p	Specific heat
C_1, C_2	Arbitrary constants
D_e	Equivalent diameter defined as $2(r_o - r_i)$
g	Gravitational acceleration
h_i	Heat transfer coefficient at the inner wall, defined by Equation (60)
k	Thermal conductivity
N_{ui}	Nusselt number at the inner wall, defined by Equation (58)
p	Static pressure of fluid in arbitrary cross section
p_o	Static pressure of fluid at pipe entrance
P	Dimensionless static pressure defined as $\frac{p}{\rho v_o^2}$
Pr	Prandtl number defined as $\frac{\mu C_p}{k}$
q	Heat flux
r	Radius from pipe center
r_i	Inner radius of annular space
r_o	Outer radius of annular space
R	Dimensionless radius defined as $\frac{r}{r_i}$

R_{max}	Dimensionless radius of maximum velocity
t	Time variable
T	Temperature
T_o	Temperature at the entrance to the annulus
T_1	Constant temperature at inner wall for case I
T_w	Wall temperature
T_b	Bulk temperature defined by Equation (55)
$\bar{T}$	Dimensionless temperature defined as $\frac{T - T_o}{T_1 - T_o}$ or $\frac{T - T_o}{q\, r_i/k}$
$\bar{T}_w$	Dimensionless wall temperature defined as $\frac{T_w - T_o}{q\, r_i/k}$
$\bar{T}_b$	Dimensionless bulk temperature
U	Dimensionless axial velocity defined as $\frac{v_z}{v_o}$
U_∞	Dimensionless fully-developed axial velocity
$(U_\infty)_{max}$	Dimensionless maximum fully-developed axial velocity
v	Velocity
v_r	Radial velocity
v_z	Axial velocity
v_o	Constant velocity at the inlet of the annulus
V	Dimensionless radial velocity defined as $\frac{v_r}{\mu/\rho r_i}$

z	Axial coordinate
Z	Dimensionless axial distance from the inlet defined as $z/\frac{v_o r_i^2 \rho}{\mu}$
Z'	Dimensionless axial distance defined as $Z/(\frac{r_o}{r_i} - 1)^2$
Z_n	Dimensionless entrance length
$\bar{Z}$	Dimensionless axial distance defined as Z/Pr

Greek symbols

μ	Viscosity
ρ	Density
θ	Polar coordinate
τ	Shear stress

ACKNOWLEDGMENTS

The author wishes to express his sincere appreciation to Dr. John C. Matthews for his help and encouragement. The author would also like to acknowledge the National Aeronautics and Space Administration for financial support and the Kansas State University Computing Center for the use of the computer.

BIBLIOGRAPHY

1. N. A. Slezkin, "Dynamics of Viscous Incompressible Fluids", in Russian, Moscow 1955, Gostechnizdat, p. 357.

2. C. C. Chang and H. B. Atabek, "Flow between Two Co-Axial Tubes near the Entry", Zeitschrift für Angewandte Mathematik und Mechanik, Vol. 42, pp. 425-430 (1962).

3. D. N. Roy, "Laminar Flow near the Entry of Coaxial Tubes", Applied Scientific Research, A - 14, pp. 421-430 (1964).

4. E. M. Sparrow and S. H. Lin, "The Developing Laminar Flow and Pressure Drop in the Entrance Region of Annular Ducts", J. of Basic Engineering, Trans. ASME, December 1964, pp. 827-834.

5. H. L. Langhaar, "Steady Flow in the Transition Length of a Straight Tube", J. of Applied Mechanics, Trans. ASME, Vol. 64, A - 55 (1942).

6. E. Sugino, "Velocity Distribution and Pressure Drop in the Laminar Inlet of a Pipe with Annular Space", Bulletin of Japanese Society of Mechanical Engineers, Vol. 5, pp. 651-655 (1962).

7. H. S. Heatons, W. C. Reynolds and W. M. Kays, "Heat Transfer in Annular Passages. Simultaneous Development of Velocity and Temperature Fields in Laminar Flow", Int. J. Heat Mass Transfer, Vol. 7, pp. 763-781 (1964).

8. K. Murakawa, "Heat Transfer in Entry Length of Double Pipes", Int. J. Heat Mass Transfer, Vol. 2, pp. 240=251 (1961).

9. R. Manohar, "An Exact Analysis of Laminar Flow in the Entrance Region of an Annular Pipe", Zeitschrift fur Angewandte Mathematik und Mechanik, 45, April 1965, pp. 171-176.

10. R. E. Lundberg, P. A. McCuen and W. C. Reynolds, "Heat Transfer in Annular Passages, Hydrodynamically Developed Laminar Flow with Arbitrarily Prescribed Wall Temperatures or Heat Fluxes", Int. J. Heat Mass Transfer, Vol. 6, pp. 495-529 (1963).

11. R. Viskanta, "Heat Transfer with Laminar Flow in Concentric Annuli with Constant and Arbitrary Variable Axial Wall Temperature", ANL - 6441, AEC Research and Development Report.

12. A. P. Hatton and A. Quarmby, "Heat Transfer in the Thermal Entry Length with Laminar Flow in an Annulus", Int. J. Heat Mass Transfer, Vol. 5, pp. 973-980 (1962).

13. C. J. Hsu and C. J. Huang, "Heat or Mass Transfer in Laminar Flow Through a Concentric Annulus with Convective Flux at Walls", Chemical Engineering Science, Vol. 21, pp. 209-221 (1966).

14. S. N. Hong, "Heat Transfer in the Thermal Entrance Region of an Annulus", M. S. Thesis, Kansas State University (1967).

15. J. L. Shohet, "Velocity and Temperature Profiles for Laminar Magneto-hydrodynamic Flow in the Entrance Region of an Annular Channel", Physics of Fluids, Vol. 5, No. 8, pp. 879-884 (August 1962).

16. J. M. Dealy, "A Neglected Effect in Entrance Flow Analyses", A. I. Ch. E. Journal, Vol. 11, No. 4, p. 745 (1965).

17. J. D. Hellums, "On a Neglected Effect in Entrance Flow Analyses", A. I. Ch. E. Journal, Vol. 12, No. 1, p. 197 (1966).

18. R. D. Richtmyer, "Difference Methods for Initial-Valued Problems", pp. 91-101, Interscience Publishers, New York (1957).

19. J. R. Bodoia, Ph. D. Thesis, Carnegie Institute of Technology, July 1959.

20. L. Lapidus, "Digital Computation for Chemical Engineers", p. 254, McGraw-Hill (1962).

21. H. S. Mickley, T. K. Sherwood and C. E. Reed, "Applied Mathematics in Chemical Engineering", p. 352, 2nd edition, McGraw-Hill (1957).

22. C. L. Hwang and L. T. Fan, "Bibliography of Hydrodynamic Entrance Region Flow", Kansas State University Bulletin, Vol. 50, No. 3, March 1966.

APPENDIX

A. The Thomas Method.

Various methods, either iterative or non-iterative, for solving systems of linear algebraic equations have been developed in the past. In obtaining the numerical solution of the present problem, the partial differential equations had been reduced by means of the finite-difference technique to a set of linear algebraic equations and the Thomas method was applied. The procedure is as follows:

Consider a system of algebraic equations with the form

$$a_1 x_1 + b_1 x_2 = d_1$$

$$c_r x_{r-1} + a_r x_r + b_r x_{r+1} = d_r \qquad r = 2, 3, \ldots, n-1$$

$$c_n x_{n-1} + a_n x_n = d_n$$

The unknowns $x_1, x_2, \ldots, x_n$ are eliminated from these equations by letting

$$w_1 = a_1$$

$$w_r = a_r - c_r q_{r-1} \qquad r = 2, 3, \ldots, n$$

$$q_{r-1} = \frac{b_{r-1}}{w_{r-1}}$$

and

$$g_1 = d_1/w_1$$

$$g_r = \frac{d_r - c_r g_{r-1}}{w_r} \qquad r = 2, 3, \ldots, n$$

Then

$$x_n = g_n$$

$$x_r = g_r - q_r x_{r+1} \qquad r = 1, 2, \ldots, n-1$$

While W, q and g are computed in the order of increasing r, the calculation of the x's is in the order of decreasing r.

An advantage of the Thomas method over the usual matrix inversion method or Gauss elimination method is that less storage space and computing time are required.

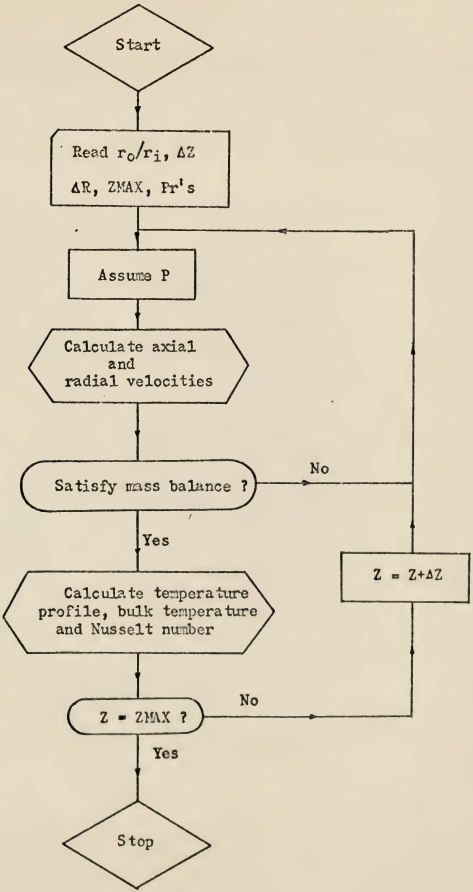

Fig. 33. Flow chart for the computer program.

B. Computer program.

```
C     THE SIMULTANEOUS DEVELOPMENT OF VELOCITY AND TEMPERATURE
C     PROFILES IN THE ENTRANCE REGION OF AN ANNULUS
      DIMENSION A(200),B(200),C(200),D(200),W(200),G(200)
      DIMENSION U(200),UN(200),V(200),VN(200),R(200),VM(200),VA(200)
      DIMENSION AA(200),BB(200),CC(200),DD(200),DDD(200),T(200),TL(200)
      DIMENSION GG(200),GGG(200),WW(200),WWW(200),T1(200),T2(200)
      DIMENSION TO1(2,200),TO2(2,200),TN1(2,200),TN2(2,200),PPR(5)
      DIMENSION UU(200),VV(200)
  100 FORMAT (6F12.6)
  200 FORMAT (I5,4F20.8)
  300 FORMAT (2F20.8)
  400 FORMAT (1H1,///3X,'PL',10X,'DELR',9X,'DELZ',9X,'Z',8X,'ITER')
  500 FORMAT (/4X,'THE AXIAL VELOCITY PROFILE UN(K)'/)
  510 FORMAT (/4X,'THE RADIAL VELOCITY PROFILE VA(K)'/)
  600 FORMAT (/4X,'ANU1',6X,'ANU2',14X,'TBU1',16X,'TBU2')
  700 FORMAT (2F10.4,2F20.8)
  800 FORMAT (4F20.8)
  900 FORMAT (4F12.6,I5)
  910 FORMAT (1H1,///5X,'DELR',8X,'DELZ',12X,'Z',7X,'PR')
  920 FORMAT (/4X,'THE TEMPERATURE PROFILE FOR CASE 1 T1(K)'/)
  922 FORMAT (/4X,'THE TEMPERATURE PROFILE FOR CASE 2 T2(K)'/)
  930 FORMAT (2F10.3)
  940 FORMAT (10F13.8)
C     CALL THE RATIO RO/RI BETA
C     ASSIGN VALUES TO BETA,DELR,DELZ,ZMAX, AND P WHERE P IS THE INLET
C     PRESSURE AND ZMAX THE MAXIMUM AXIAL DISTANCE
      READ (1,100) BETA,DELR,DELZ,DELY,ZMAX,P
      READ (1,930) (PPR(K),K=1,2)
      L=0
      Z=0.0
      AN=(BETA-1.)/DELR
      N=AN
      NN=N+1
      MM=N-1
      MA=N-2
C     AT THE POINTS OF CONTINUITY, SET
      U(1)=0.5
      U(NN)=0.5
      T(1)=0.5
      T(NN)=0.0
      TL(1)=0.0
      TL(NN)=0.0
      TO1(1,1)=0.5
      TO1(2,1)=0.5
      TO2(1,1)=0.0
      TO2(2,1)=0.0
C     THE BOUNDARY CONDITIONS ARE
      DO 1 J=1,2
      DO 1 K=2,NN
      TO1(J,K)=0.0
      TO2(J,K)=0.0
```

```
    1 CONTINUE
      DO 2 K=2,N
      U(K)=1.0
      T(K)=0.0
    2 TL(K)=0.0
C     THE MATERIAL BALANCE
      XX=(BETA*BETA-1.)/(2.*DELR)
C     CALCULATION OF RADIAL POSITIONS
      DO 3 K=1,NN
      V(K)=0.0
      AK=K
    3 R(K)=1.+(AK-1.)*DELR
      DN=DELR*DELR/DELZ
C     ASSUME A REASONABLE VALUE FOR THE PRESSURE
      PN=9.993286
   15 CONTINUE
      ITER=1
      MX=-5
      L=L+1
      Z=Z+DELZ
      IF(Z.GT.ZMAX) GO TO 90
      IF(L-1) 13,13,44
   13 DO 14 K=1,NN
      UU(K)=U(K)
   14 VV(K)=V(K)
   44 CONTINUE
C     NAME THE PRANDTL NUMBER PR
      PR=0.01
C     CALCULATION OF THE COEFFICIENTS IN THE ORDER OF INCREASING R
C     FOR THE TEMPERATURE PROFILES
      DO 40 K=2,N
      AA(K)=2./PR+DN*U(K)
      BB(K)=DELR*V(K)/2.-DELR/(2.*R(K)*PR)-1./PR
      CC(K)=DELR/(2.*R(K)*PR)-DELR*V(K)/2.-1./PR
   40 DD(K)=DN*U(K)*T(K)
      WW(2)=AA(2)
      GG(2)=(DD(2)-CC(2))/WW(2)
      DO 50 K-3,MM
      WW(K)=AA(K)-CC(K)*BB(K-1)/WW(K-1)
      GG(K)=(DD(K)-CC(K)*GG(K-1))/WW(K)
      IF(GG(K).LT.0.00000001) GG(K)=0.0
   50 CONTINUE
      WW(N)=AA(N)+BB(N)-CC(N)*BB(N-1)/WW(N-1)
      GG(N)=(DD(N)-CC(N)*GG(N-1))/WW(N)
      DO 88 K=2,N
   88 DDD(K)*=DN*U(K)*TL(K)
      WWW(2)=CC(2)+AA(2)
      GGG(2)=(DDD(2)-CC(2)*DELR*(1.-0.5*DELR))/WW(2)
      DO 99 K=3,MM
      WWW(K)=AA(K)-CC(K)*BB(K-1)/WWW(K-1)
      GGG(K)=(DDD(K)-CC(K)*GGG(K-1))/WWW(K)
      IF(GGG(K).LT.0.00000001) GGG(K)=0.0
   99 CONTINUE
      WWW(N)=AA(N)+BB(N)-CC(N)*BB(N-1)/WWW(N-1)
      GGG(N)=(DDD(N)-CC(N)*GGG(N-1))/WWW(N)
```

```
C     SOLUTION OF THE VELOCITY PROFILE BY THE THOMAS METHOD
      PL=PN
      DO 4 K=2,N
      A(K)=2.+DN*U(K)
      B(K)=V(K)*DELR/2.-1.-DELR/(2.*R(K))
    4 C(K)=DELR/(2.*R(K))-1.-V(K)*DELR/2.
   22 CONTINUE
      DO 5 K=2,N
    5 D(K)=DN*P+DN*U(K)*U(K)-DN*PL
      W(2)=A(2)
      DO 6 K=3,N
      W(K)=A(K)-C(K)*B(K-1)/W(K-1)
    6 G(K)=(D(K)-C(K)*G(K-1))/W(K)
C     THE AXIAL VELOCITIES AT WALLS ARE ZERO
      UN(1)=0.0
      UN(NN)=0.0
C     THE VELOCITY IS CALCULATED IN THE ORDER OF DECREASING R
      UN(N)=G(N)
      DO 7 K=1,MA
      I=N-K
    7 UN(I)=G(I)-UN(I+1)*B(I)/W(I)
      SUMU=0.0
      DO 8 K=2,N
    8 SUMU=SUMU+R(K)*UN(K)
C     THE PRESSURE IS DETERMINED IN SUCH A MANNER THAT AN ERROR OF
C     ±0.01% IS ALLOWED FOR THE MATERIAL BALANCE
      IF(ABS(XX-SUMU)-0.04) 55,55,77
   77 CONTINUE
      IF(MX) 70,70,80
   70 IF(XX-SUMU) 80,55,75

   75 PL=PL-0.001
      ITER=ITER+1
      GO TO 22
   80 IF(XX-SUMU) 85,55,95
   85 PL=PL+0.0001
      ITER=ITER+1
      MX=5
      GO TO 22
   95 PL=PL-0.00001
      ITER=ITER+1
      GO TO 22
   55 CONTINUE
C     CALCULATION OF RADIAL VELOCITY FROM EQUATION OF CONTINUITY
C     RADIAL VELOCITIES AT WALLS ARE ZERO
      VN(1)=0.0
      VN(NN)=0.0
      DO 18 K=1,MM
   18 VN(K+1)=R(K)*VN(K)/R(K+1)-(DELR/(2.*R(K+1)*DELZ))*(R(K+1)*(UN(K+1)
     1-U(K+1))+R(K)*(UN(K)-U(K)))
C     THE BIASED DOWNWARD VELOCITY DISTRIBUTION
      VM(1)=0.0
      VM(NN)=0.0
      DO 19 K=1,MM
```

```
      I=NN-K
   19 VM(I)=R(I+1)*VM(I+1)/R(I)+(DELR/(2.*R(I)*DELZ))*(R(I)*(UN(I)=U(I))
     1+R(I+1)*(UN(I+1)-U(I+1)))
C     CALCULATION OF THE AVERAGE RADIAL VELOCITIES
      VA(1)=0.0
      VA(NN)=0.0
      VA(2)=VN(2)
      VA(N)=VM(N)
      DO 21 K=3,MM
   21 VA(K)=(VN(K)+VM(K))/2.
C     THE TEMPERATURE PROFILES
C     CASE 1 -- CONSTANT TEMPERATURE AT THE INNER WALL AND OUTER WALL
C                INSULATED
C     THE WALL TEMPERATURE IS ALWAYS UNITY
      T1(1)=1.0
C     THE TEMPERATURE DISTRIBUTION IS CALCULATED IN THE ORDER OF
C     DECREASING R
      T1(NN)=GG(N)
      T1(N)=GG(N)
      DO 60 K=1,MA
      I=N-K
   60 T1(I)=GG(I)-T1(I+1)*BB(I)/WW(I)
      SUMT1=0.0
      DO 66 K=2,N
   66 SUMT1=SUMT1+UN(K)*T1(K)*R(K)
C     EVALUATION OF THE AVERAGE TEMPERATURE AND NUSSELT NUMBER
      TBU1=2.*DELR*SUMT1/(BETA*BETA-1.)
      ANU1=2.*(BETA-1.)*(T1(1)-T1(2))/(DELR*(1.-TBU1)*(1.-DELR/2.))
C     CASE 2 -- CONSTANT FLUX AT THE INNER WALL AND OUTER WALL INSULATED
      T2(NN)=GGG(N)
      T2(N)=GGG(N)
      DO 101 K=1,MA
      I=N-K
  101 T2(I)=GGG(I)-T2(I+1)*BB(I)/WWW(I)
      T2(1)=T2(2)+DELR*(1.-0.5*DELR)
C     EVALUATION OF BULK TEMPERATURE AND NUSSELT NUMBER
      TBU2=2.*Z/(PR*(BETA*BETA-1.))
      ANU2=2.*(BETA-1.)/(T2(1)-TBU2)
      IF(L-6) 122,205,205
  122 CONTINUE
      DO 120 K=1,NN
      U(K)=UN(K)
      V(K)=VA(K)
      T(K)=T1(K)
  120 TL(K)=T2(K)
      P=PL
      PN=PL-0.00014
      GO TO 15
  205 CONTINUE
      WRITE (3,400)
      WRITE (3,900) PL,DELR,DELZ,Z,ITER
      WRITE (3,500)
```

```
      DO 121 K=1,NN
      WRITE (3,200) K,UN(K),VA(K),T1(K),T2(K)
  121 CONTINUE
      WRITE (3,600)
      WRITE (3,700) ANU1,ANU2,TBU1,TBU2
C     TEMPERATURE PROFILES FOR PR=1.0 AND 10.0
      DM=DELR*DELR/DELY
      DO 999 L=1,2
      PR=PPR(L)
      DO 210 K=2,N
      AA(K)=2./PR+DM*UU(K)
      BB(K)=DELR*VV(K)/2.-DELR/(2.*R(K)*PR)-1./PR
      CC(K)=DELR/(2.*R(K)*PR)-DELR*VV(K)/2.-1./PR
  210 DD(K)=DM*UU(K)*TO1(L,K)
      WW(2)=AA(2)
      GG(2)=(DD(2)-CC(2))/WW(2)
      DO 220 K=3,MM
      WW(K)=AA(K)-CC(K)*BB(K-1)/WW(K-1)
      GG(K)=(DD(K)-CC(K)*GG(K-1))/WW(K)
      IF(GG(K).LT.0.00000001) GG(K)=0.0
  220 CONTINUE
      WW(N)=AA(N)+BB(N)-CC(N)*BB(N-1)/WW(N-1)
      GG(N)=(DD(N)-CC(N)*GG(N-1))/WW(N)
      DO 230 K=2,N
  230 DDD(K)=DM*UU(K)*TO2(L,K)
      WWW(2)=CC(2)+AA(2)
      GGG(2)=(DDD(2)-CC(2)*DELR*(1.-0.5*DELR))/WWW(2)
      DO 240 K=3,MM
      WWW(K)=AA(K)-CC(K)*BB(K-1)/WWW(K-1)
      GGG(K)=(DDD(K)-CC(K)*GGG(K-1))/WWW(K)
      IF(GGG(K).LT.0.00000001) GGG(K)=0.0
  240 CONTINUE
      WWW(N)=AA(N)+BB(N)-CC(N)*BB(N-1)/WWW(N-1)
      GGG(N)=(DDD(N)-CC(N)*GGG(N-1))/WWW(N)
      TN1(L,1)=1.0
      TN1(L,NN)=GG(N)
      TN1(L,N)=GG(N)
      DO 250 K=1,MA
      I=N-K
  250 TN1(L,I)=GG(I)-TN1(L,I+1)*BB(I)/WW(I)
      SUMTN1=0.0
      DO 260 K=2,N
  260 SUMTN1=SUMTN1+UN(K)*R(K)*TN1(L,K)
      TBU1=2.*DELR*SUMTN1/(BETA*BETA-1.)
      ANU1=2.*(BETA-1.)*(TN1(L,1)-TN1(L,2))/(DELR*(1.-TBU1)*(1.-DELR/2.))
      TN2(L,NN)=GGG(N)
      TN2(L,N)=GGG(N)
      DO 270 K=1,MA
      I=N-K
  270 TN2(L,I)=GGG(I)-TN2(L,I+1)*BB(I)/WWW(I)
      TN2(L,1)=TN2(L,2)+DELR*(1.-0.5*DELR)
```

```
      TBU2=2.*Z/(PR*(BETA*BETA-1.))
      ANU2=2.*(BETA-1.)/(TN2(L,1)-TBU2)
      WRITE (3,910)
      WRITE (3,100) DELR,DELY,Z,PR
      WRITE (3,920)
      DO 275 K=1,NN
  275 WRITE (3,940) K,TN1(L,K),TN2(L,K)
      WRITE (3,600)
      WRITE (3,700) ANU1,ANU2,TBU1,TBU2
      DO 310 K=1,NN
      TO1(L,K)=TN1(L,K)
  310 TO2(L,K)=TN2(L,K)
      IF(Z-0.00024) 999,999,280
  280 DO 290 K=1,NN
  290 PUNCH 300,TN1(L,K),TN2(L,K)
  999 CONTINUE
      DO 320 K=1,NN
      U(K)=UN(K)
      V(K)=VA(K)
      T(K)=T1(K)
  320 TL(K)=T2(K)
      L=0
      P=PL
      PN=PL-0.00014
      IF(Z-0.00024) 15,15,33
   33 DO 125 K=1,NN
  125 PUNCH 800,UN(K),VA(K),T1(K),T2(K)
      GO TO 15
   90 STOP
      END
```

ANNULAR HEAT TRANSFER WITH SIMULTANEOUSLY DEVELOPING VELOCITY AND TEMPERATURE PROFILES

by

KHANH-DAN HA

B.S., Cheng Kung University, 1966

AN ABSTRACT OF A MASTER'S THESIS

submitted in partial fulfillment of the

requirements for the degree

MASTER OF SCIENCE

Department of Chemical Engineering

KANSAS STATE UNIVERSITY
Manhattan, Kansas

1969

ABSTRACT

A numerical analysis is made of the problem of simultaneously developing velocity and temperature profiles of a Newtonian fluid in the entrance region of an annulus. The flow is assumed laminar and the fluid to possess constant physical properties. Two distinct cases are considered in this study:

(i) Constant temperature at the inner surface, outer surface insulated,

(ii) Constant heat flux at the inner surface, outer surface insulated.

Results are presented for Prandtl numbers of 0.01, 1.0 and 10.0 and for values of the ratio of outer to inner radii of 2.0 and 10.0. Comparisons, when possible, have been made with results obtained by other investigators.